E-269

MR No. E5J02

NATIONAL ADVISORY COMMITTEE FOR AERONAUTICS

WARTIME REPORT

ORIGINALLY ISSUED

October 1945 as
Memorandum Report E5J02

SEA-LEVEL PERFORMANCE TESTS OF A 22-INCH-DIAMETER PULSE-JET ENGINE AT VARIOUS SIMULATED RAM PRESSURES

By Eugene J. Manganiello, Michael F. Valerino
and Robert H. Essig

Aircraft Engine Research Laboratory
Cleveland, Ohio

NACA

WASHINGTON

NACA MR No. E5J02

NATIONAL ADVISORY COMMITTEE FOR AERONAUTICS

MEMORANDUM REPORT

for the

Air Technical Service Command, Army Air Forces

and the

Bureau of Aeronautics, Navy Department

SEA-LEVEL PERFORMANCE TESTS OF A 22-INCH-DIAMETER PULSE-JET ENGINE AT VARIOUS SIMULATED RAM PRESSURES

By Eugene J. Manganiello Michael F. Valerino
and Robert H. Essig

SUMMARY

Results are presented of sea-level performance tests conducted on a 22-inch-diameter pulse-jet engine installed on a thrust stand. The tests were conducted at simulated ram pressures of 0, 18, 40, and 58 inches of water and cover the entire range of fuel flows for which resonant operation of the engine is obtained.

A summary of the important test results is presented in the following table:

Simulated ram pressure, in. water	0	18	40	58
Equivalent indicated airspeed (NACA air), mph	0	190	280	340
Predicted maximum flight thrust, lb	500	660	740	770
Thrust specific fuel consumption at maximum-thrust operation, lb/(hr)(lb thrust)	4.0	3.8	3.8	4.2
Predicted flight thrust for operation at minimum fuel consumption, lb	420	610	660	680
Minimum value of thrust specific fuel consumption, lb/(hr)(lb thrust)	3.8	3.4	3.3	3.6

Maximum-thrust operation was obtained at a fuel-air ratio of approximately 0.08 and best fuel economy, in the fuel-air-ratio range between 0.064 and 0.072.

The operating frequency of the engine varied from 39 to 41 cycles per second. Maximum combustion-chamber pressures in the order of 40 to 50 inches of mercury gage and minimum pressures from about 7 to 10 inches of mercury vacuum were measured for the simulated ram pressures of 40 and 58 inches of water. The operating lives of the two flapper-valve assemblies used in the tests were approximately 17 and 33 minutes.

INTRODUCTION

At the request of the Air Technical Service Command, Army Air Forces, and the Bureau of Aeronautics, Navy Department, an investigation is being conducted at the NACA Cleveland laboratory to improve the performance and extend the operating life of the pulse-jet engine. As a part of this investigation, thrust-stand tests were conducted to determine the sea-level performance of a 22-inch-diameter pulse-jet engine at simulated ram pressures of 0, 18, 40, and 58 inches of water for the entire fuel-flow range of resonant operation. The performance data obtained in these tests, which were conducted from February to June 1945, are presented in this report.

TEST INSTALLATION AND INSTRUMENTATION

Description of pulse-jet engine and its operation. - The pulse-jet engine used in the investigation is a reproduction of the German engine used in World War II for propelling the V-1 flying bomb. As illustrated in the dimensioned sketch of figure 1, the pulse-jet engine consists of a flapper-valve grid assembly and a steel shell that forms the diffuser entry ahead of the grid, the cylindrical combustion chamber, the conical nozzle, and the long cylindrical tail pipe behind the grid. The inner diameters of the combustion chamber and tail pipe are $21\frac{1}{2}$ and $15\frac{1}{8}$ inches, respectively; the ratio of combustion chamber to tail-pipe flow area is therefore approximately 2:1. The flapper-valve grid assembly consists of spring-steel sheets 0.010 inch thick, which are preformed and installed to seat tightly against the ribs of the aluminum grid sections. (See detailed sketch in fig. 1.) The spaces between the ribs form the air passages across the grid sections; the restriction of air flow through these passages is controlled by the opening and closing action of the flapper valves. Three horizontal venturi-shaped channels are located at the entrance to the combustion chamber directly downstream of the flapper-valve grid assembly. The venturi channels are formed by the insertion in the forward end of the combustion chamber of airfoil sections constructed of sheet metal. The spray ends of the fuel nozzles, which are supported on the flapper-valve grid assembly, are centrally located slightly upstream of the throat of the venturi channels. The purpose of these

channels is probably to improve mixing between the combustion air and the fuel. A spark plug installed on the combustion-chamber shell in the position indicated in figure 1 is used for starting the engine.

Figures 2 and 3 are photographs of the downstream and upstream faces of the flapper-valve grid assembly and show the nine centrifugal-spray fuel-injection nozzles, the three compressed-air jets, the fuel-distribution manifold, and the compressed-air lines. The compressed-air jets, which are incorporated for static starting, were not used in the tests.

Resonant operation of the engine is as follows: The flapper valves open and admit air into the combustion chamber. The fuel spray mixes with the incoming air and forms a combustible mixture, which is ignited by the residual exhaust gases of the previous explosion. The pressure rise resulting from the explosive combustion causes the flapper valves to snap shut against the grid and the burned products of combustion are discharged rearwardly through the tail pipe, thus providing a thrust impulse on the engine in a forward direction. The outward rush of gases from the tail pipe reduces the pressure within the combustion chamber, which causes the flapper valves to reopen and admit a new charge of air. The cycle then repeats itself at a frequency governed by the resonant frequency of the engine tube.

Thrust stand and thrust-measuring system. - Figure 4 is a schematic diagram of the test setup showing the mounting frame, the thrust platform and thrust-measuring linkage, and the general ducting system for supplying combustion air to the engine. The shrouds and ducting of the cooling-air system and other details of the test installation may be seen in the photograph of figure 5. The front (upstream) support for the engine consists of an adjustable yoke having flexible rubber-mounted bearings at the two support points for cushioning the violently fluctuating thrust forces obtained during operation. The rear (downstream) support is fixed to the frame with a simple sliding bolt and slot arrangement to provide for the expansion of the shell when heated during normal operation. After initial tests, the extreme end of the tail pipe was clamped to the frame by means of metal straps to prevent it from whipping and sagging during operation. The thrust platform, upon which the mounting frame is bolted, is supported by ball and roller bearing linkages above a bedplate securely anchored to an isolated concrete block set in the ground.

The thrust platform, the support linkages, and the bedplate form the sides of a pin-jointed parallelogram. The rear support linkages and a thrust arm are keyed to a common shaft to form a bell-crank arrangement with a 10:1 leverage ratio. The forces on the engine are transmitted from the thrust platform, through the bell crank, to the piston of a hydraulic piston-cylinder assembly. Kerosene is

pumped from a reservoir to the bottom of the cylinder and returned through a horizontal slot 1/16 inch wide and 7/8 inches long midway in the cylinder barrel. Under load conditions the piston automatically assumes a position relative to the slot opening such that the kerosene pressure exerted on the under side of the piston balances the forces applied to the top of the piston. The kerosene pressure in the cylinder is transmitted to a mercury manometer through copper tubing, which incorporates a 1-foot length of capillary tubing with a 0.032-inch inside diameter. The capillary tubing provides for linear damping of the pressure pulsations resulting from the intermittent jet forces and thus insures true time-average readings.

In order to check the accuracy and reliability of the thrust readings obtained with this hydraulic-balance system, thrust measurements were also taken in some tests (not reported herein) with a strain gage installed on the connecting rod between the thrust arm and the balancing piston. Agreement between the thrust indications obtained by the two methods were within 5 percent; because the two thrust-measuring methods operate on entirely different principles, insofar as giving a time average of the periodic thrust forces developed by the engine, it is concluded that the time-average thrust measurements obtained by either method are correct.

Combustion-air system. - As shown in figure 4, a centrifugal blower driven through a variable-speed magnetic coupling by a 200-horsepower constant-speed induction motor supplies combustion air to a large surge tank from which it flows to the pulse-jet engine. The surge tank, which serves as a constant-pressure reservoir, has a volume greater than 300 times the volume of the engine combustion chamber; the air-pressure fluctuations in the surge tank, resulting from the cyclic "breathing" of the engine, are therefore small. An air-tempering tank, located in the ducting system between the blower outlet and the air surge tank, contains suitable steam coils and water coils with automatically controlled mixing vanes for regulation of the combustion-air temperature. The surge-tank pressure (or simulated ram pressure) was controlled by regulation of the blower speed and a bleed valve located near the blower outlet. Measurements of combustion-air weight flow were obtained by means of a 14-inch thin-plate orifice installed in the combustion-air system according to A.S.M.E. specifications.

The transition ducting between the air surge tank and the entrance diffuser of the engine is rigidly supported on the same mounting frame as the engine itself and is connected to the surge tank by means of a flexible rubber diaphragm (see detail A, fig. 4), which prevents transmittal of thrust to the surge tank. Because the engine mounts permit some movement of the engine relative to the mounting frame, whereas the transition ducting is rigidly fastened

to the frame, a rubber-boot connection is provided between the engine diffuser and the transition section (see detail B, fig. 4).

Fuel and ignition systems. - Fuel, conforming to AN-F-22 specifications, was piped to the engine from the laboratory main supply system. An auxiliary fuel pump was used to boost the main-supply fuel pressures, as required to obtain the high fuel rates and the attendant high fuel-nozzle pressures. The fuel flow was regulated by a needle valve and measured by a calibrated rotameter. A solenoid-operated valve in the fuel line adjacent to the engine afforded a quick means of opening and shutting off the fuel supply to the engine during operation. A fuel surge tank is connected by a tee from the fuel line at a point just upstream of the solenoid-operated valve. The volume in the lower portion of the tank nearest the connection is filled with gasoline and the upper volume contains entrapped air for cushioning the line surges. The fuel surge tank also functioned in starting the engine as a pressurized fuel reservoir for giving a quick high-pressure injection of fuel into the combustion chamber the instant the solenoid valve was opened.

A 10,000-volt output transformer and a 14-millimeter automobile-engine spark plug provided the initial ignition required for starting the engine.

Cooling-air system. - The engine is cooled during operation by circulation of cooling air in the annular space between the engine shell and the cooling shrouds shown in figure 5. The cooling air is delivered to the cooling shrouds by a centrifugal blower driven through a hydraulic coupling by a 900-horsepower constant-speed induction motor. The cooling-shroud installation is not in contact with the engine or the thrust-transmitting members and thus does not interfere with the thrust measurements. The cooling air is introduced into and discharged from the annular space in such a manner that its total momentum along the thrust axis of the engine is kept at a minimum.

Pressure and temperature measurements. - The pressure-tube and thermocouple instrumentation used in the tests is briefly outlined as follows:

(a) A survey with four total-pressure tubes at the engine diffuser entrance (plane h, fig. 6). The average pressure above atmospheric thus obtained would correspond closely to flight ram pressure.

(b) A survey with four static tubes and four iron-constantan thermocouples at the surge tank outlet (plane i, fig. 6).

(c) Static-pressure wall tap for measurement of the static pressure of the combustion air within the air surge tank.

(d) Flange static taps upstream and downstream and an iron-constantan thermocouple upstream of the combustion-air orifice plate. These readings are used for the determinations of combustion-air flow.

(e) Three iron-constantan thermocouples peened into the upstream face of the flapper-valve assembly.

(f) Five chromel-alumel thermocouples spot-welded to the engine shell at 2-foot intervals downstream of the flapper-valve assembly.

The pressure tubes are connected to a multitube liquid manometer, the readings of which were photographically recorded during the tests. A micromanometer was used to obtain a more accurate reading of the combustion-air pressure differential across the orifice plate. The temperatures were indicated by self-balancing potentiometers.

Combustion-cycle measurements. - The engine combustion-chamber pressures were transmitted to a capacity-type pressure pickup and were obtained as vertical deflections on a cathode-ray oscilloscope. The horizontal sweep on the oscilloscope was actuated by a calibrated audio-frequency oscillator, which resulted in a trace on the oscilloscope screen of pressure against time. The pressure trace on the screen was photographed during the tests. The frequency of the pressure trace was obtained from the setting of the audio-frequency oscillator.

Preliminary tests showed that the pressure pickup was relatively insensitive to vibrational disturbances, but that, in spite of its water-cooled pressure-sensitive diaphragm, it gave highly distorted and changing wave forms when subjected to hot gases. This response may be due to warping and changes in the physical properties of the thin diaphragm upon application of heat. In order to avoid direct exposure of the diaphragm to the combustion gases, the pickup was installed at the end of a water-cooled extension tube of 3/8-inch inside diameter and 3$\frac{1}{2}$-inch length, which, in turn, was mounted on the combustion chamber about 1 foot behind the flapper-valve assembly.

The quantitative information on the combustion pressure cycle is obtained from measurements of maximum and minimum cycle pressures. A balanced-disk pickup of NACA design, which has been successfully used in reciprocating-engine development to measure maximum cylinder pressures and found to be reliable, was used in the subject tests to measure the maximum cycle pressure. In the operation of the

balanced-disk pickup the cyclic combustion pressure acting on one side of the disk is counteracted by a controllable constant air pressure on the opposite side. The counteracting pressure, when adjusted to the lowest value that will keep the disk on its seat at all times, will be closely equal to the maximum combustion pressure. This condition of balance is indicated by a 1-watt neon lamp in a direct-current circuit that includes the disk and its seat. The pressure pickup used for measuring minimum pressure is similar in construction and operation to that described for measuring maximum pressure; the balancing constant pressure in this case is maintained by a vacuum pump.

ANALYSIS OF TEST DATA

In order to interpret the test results for application to the conditions of flight, a brief theoretical study is given of the air flow and the resulting forces present both in flight and in the test installation. Figure 6(a) illustrates the flow conditions existing when the engine is in flight. Momentum considerations of the flow through the imaginary boundary drawn in figure 6(a) results in the following relation:

$$F = \frac{W}{g} (V_j - V_o) \qquad (1)$$

where

F average thrust developed by engine, pounds

W combustion-air weight flow through engine, pounds per second

g acceleration of gravity, 32.2 feet per second per second

V_j effective jet velocity equal to momentum of exhaust jet divided by mass flow of combustion air, feet per second

V_o free-stream velocity, feet per second

The flow conditions obtained in the tests (see fig. 6(b)) are somewhat different from those existing in flight. In this case, the momentum equation when applied to the flow through the imaginary boundaries yields:

$$F_m = A_i (p_o - p_i) + \frac{W}{g} (V_j - V_i) \qquad (2)$$

where

F_m force measured in tests, pounds

A_i area effective in transmitting air load $p_i - p_o$ to engine and supporting structure, square inches

p_o atmospheric pressure, pounds per square inch

p_i average static pressure inside surge tank at cross section of area A_i, pounds per square inch

V_i effective air velocity at cross section of area A_i, feet per second

It is noted that the imaginary boundary passes through the crest of the flexible rubber diaphragm. At this point the tension in the diaphragm is normal to the axis of the engine and hence does not contribute a term to equation (2).

Equation (2) shows that the total force measured in the tests is the algebraic summation of the air-pressure load $A_i (p_o - p_i)$ and the momentum force $\frac{W}{g}(V_j - V_i)$. The air-pressure load may be evaluated from the results of calibration tests, which are described later. The momentum term $\frac{W}{g} V_i$ is determined from the measured value of combustion-air weight flow and the value of V_i, which, in turn, is obtained from the calculated average velocity at plane i (fig. 6) by assuming the velocity variation resulting from the cyclic-flow through the engine to be sinusoidal. Because the average velocity at plane i (fig. 6) is small (less than 1 percent of V_j), the foregoing approximation for V_i introduces negligible error. The measured test force F_m may then be corrected by the values of $A_i (p_o - p_i)$ and $\frac{W}{g} V_i$ in accordance with equation (2) to give the jet momentum force $\frac{W}{g} V_j$, herein referred to as the jet thrust.

For convenience of analysis, the effective jet velocity V_j is calculated from the jet thrust $\frac{W}{g} V_j$ and the combustion-air weight flow W. The engine performance results are then presented as plots of effective jet velocity and combustion-air weight flow against fuel flow for the various simulated ram pressures. Predicted flight thrust values (excluding external drag) for the airspeeds corresponding to the simulated ram pressures are presented as computed from equation (1) and the test values of effective jet velocity and combustion-air weight flow.

The foregoing procedure involves the assumption that, for the same conditions of fuel flow and entrance ram pressure and temperature, the combustion-air weight flow and the effective jet velocity (and thus, the jet thrust) are the same for the engine in flight as on the thrust stand. The main implications of this assumption are that the combustion-air weight flow and the effective jet velocity are unaffected by the cyclic disturbances of the air stream ahead of the engine entrance diffuser and by the flow of slipstream along the engine shell, as obtained in flight.

TEST PROCEDURE

Thrust-calibration tests. - The thrust-measuring system was calibrated previous to the tests to determine:

(a) The conversion factor between thrust-manometer deflection and net force F_m on the engine structure.

(b) The air load $A_i (p_i - p_o)$ on the engine structure at the various static-pressure values $(p_i - p_o)$ used in the tests.

The calibrating rig consisted of a weight-loading pan connected to the thrust platform with a steel cable running over a separately supported pulley. During the calibration tests the tail-pipe outlet of the jet engine was plugged; the static pressure within the surge tank and the engine was then built up with the combustion-air blower.

Engine-performance tests. - In order to start the engine, a simulated ram pressure of 20 inches of water was maintained in the air surge tank and a fuel pressure of 15 pounds per square inch gage was built up in the fuel surge tank. The fuel solenoid valve was then opened and immediately thereafter the spark was energized. Following the first explosion the spark was deenergized and the needle valve in the fuel line was rapidly opened to provide the required fuel flow for the greatly increased air flow induced by the breathing action of the engine. Predetermined values of simulated ram pressure and fuel flow (range of fuel flows limited to that resulting in resonant operation) were set and the engine operating conditions were allowed to stabilize before start of the test run. During the test run, which was of approximately 30 seconds duration, the pertinent test data were recorded; the thrust-manometer reading was taken at the end of the 30-second run period. Upon completion of the first test run, new fuel-flow and simulated ram-pressure conditions were established and the procedure for recording the data was repeated. The running time per start was limited by the temperature of the engine shell (1600° F chosen as a maximum limit) that could not be adequately cooled with the available cooling

air (approximately 10 to 12 lb/sec). Only two and sometimes three test runs could be made with a single test start; after these runs it was necessary to shut down to allow the engine shell to cool.

A summary of the simulated ram pressures and fuel flows used in tests with two standard flapper-valve assemblies is given in the following table:

Simulated ram pressure, in. water			
0	18	40	58
Fuel flow, lb/hr			
1600	1600	1800	2200
1800	2000	2000	2400
2000	2200	2400	2500
2200	2400	2800	2800
		3000	3200
		3200	3500

In these tests, the combustion-air temperature was maintained constant at approximately 70° F.

Steady-flow pressure-loss tests. - The relation between air weight flow and pressure drop across the flapper-valve assembly was determined in steady air-flow tests conducted prior to operation of the engine. In these tests, air was pumped by the combustion-air blower to the flapper-valve assembly from where it flowed as a steady stream into the engine shell and out to the atmosphere. The air flow was varied in steps from the lowest value that could be reliably measured with the combustion-air orifice to the maximum quantity safely pumped by the combustion-air blower; measurements were taken of the air weight flow and of the difference between the air pressure within the surge tank and the atmospheric pressure, which is approximately equal to the static pressure drop across the flapper-valve assembly.

Fuel-nozzle calibration tests. - Previous to the tests, the fuel-manifold-injection-nozzle assembly was calibrated to determine the fuel distribution among the nine fuel-injection nozzles at fuel-nozzle pressures of 5, 10, 15, 20, and 25 pounds per square inch gage (upper limit of the flow-bench equipment). This calibration was conducted with the fuel manifold in the same vertical position as installed on the engine; at each fuel pressure tested the fuel flow issuing from each injection nozzle was separately measured. The results of these fuel-distribution tests, as conducted on the

second flapper-valve assembly, are given in figure 7 where the individual fuel flow is plotted for each nozzle. Included in the figure is a sketch that identifies the nozzle number and shows the position of the nozzle on the grid. The percentage deviations from the average fuel flow and the total fuel flow for each fuel pressure are also listed on the figure.

RESULTS AND DISCUSSION

A summary of the performance results obtained in the tests with the two standard flapper-valve assemblies is presented in tables I and II.

Combustion-air flow and effective jet velocity. - The basic over-all performance of the engine is presented in figures 8 and 9, wherein the combustion-air weight flow and the effective jet velocity, respectively, are plotted against fuel flow for simulated ram pressures of 0, 18, 40, and 58 inches of water. The end test points on each ram-pressure curve in figure 9 represent the limits of the jet-engine cycling or resonating operation; a small reduction in fuel flow (about 100 to 200 lb/hr) below the lower test limit or increase above the upper test limit resulted in a change in combustion to steady burning, for which the effective jet velocity is only a very small fraction of that developed during resonant operation.

Figures 8 and 9 show that, for a ram pressure of 0, from 6 to 7 pounds per second of air is induced into the engine for combustion, upon which an effective jet velocity of about 2300 feet per second is developed. This static performance is possible only because of the resonant pressure variations occurring within the engine during its operation; the induction of air is due, in this case, solely to the suction pressures created within the engine after each cycle explosion, whereas the high velocity discharge is the result of the rapid build-up of pressure during the combustion process.

The combustion-air weight flow increases with increase in both fuel flow and ram pressure (fig. 8); at the maximum simulated ram pressure of 58 inches of water, the combustion-air weight flow is close to 12 pounds per second. Based on the assumption that owing to the flapper-valve action the induction period in each cycle is half the total cycle time, this air flow corresponds to an average air velocity during the induction period of about 360 feet per second through the throat of the venturi passages. The engine volumetric efficiency corresponding to this air flow is about 38 percent, as based on a cycling rate of 40 cycles per second (see tables I and II) and the engine volume between the flapper-valve assembly and the throat of the convergent nozzle (beginning of the constant-area tail pipe).

Figure 9 shows that, as the fuel flow is increased from the lower to the upper cycling limit at each ram pressure, the effective jet velocity increases to a maximum value and then decreases. The maximum effective jet velocity is seen to increase substantially when the ram pressure is changed from 0 to 18 inches of water. Throughout the range of ram pressures from 18 to 58 inches of water, however, the maximum effective jet velocity varies only about 140 feet per second and appears to be highest at a ram pressure of 40 inches of water.

The effective jet velocity is plotted in figure 10 against fuel-air ratio as obtained from the test points presented in figures 8 and 9. The fairing of the curves through the test points in this and subsequent figures was made in a manner to give consistent results with the basic curves of figures 8 and 9. The effective jet velocity is shown to be a maximum in the vicinity of 0.08 fuel-air ratio for all the ram pressures tested.

Predicted flight thrust. - The thrust that would be developed in sea-level flight for the atmospheric pressure and temperature test conditions (approximately NACA air) at the flight speeds corresponding to the test simulated ram pressures are plotted against fuel flow in figure 11 and against fuel-air ratio in figure 12. Because the effect of altitude on the engine performance is not known, figures 11 and 12 are presented for only sea-level operation. A variation of about 16 percent exists between the maximum static thrust (at 0 ram) and the thrust developed at 190 and 280 miles per hour at the same fuel flow. The maximum thrust increases with airspeed at a rapidly decreasing rate; for airspeeds of 0, 190, 280, and 340 miles per hour, the maximum thrust values are 500, 660, 740, and 770 pounds, respectively. It is evident from figures 11 and 12 that, although the fuel flow for maximum thrust increases with increase in airspeed, the air flow increases in the same proportion so that in every case maximum thrust occurs at a fuel-air ratio of about 0.08.

Fuel consumption. - The thrust specific fuel consumption of the engine in pounds of fuel per hour per pound thrust (excluding external drag) is plotted in figure 13 against fuel-air ratio for the various indicated airspeeds. Best-economy operation is obtained at a fuel-air ratio of 0.064 for flight speeds of 280 and 340 miles per hour and at a fuel-air ratio of about 0.072 for flight speeds of 0 and 190 miles per hour. The thrust specific fuel consumption for best-economy operation at flight speeds of 0, 190, 280, and 340 miles per hour are, respectively, 3.8, 3.4, 3.3, and 3.6 pounds of fuel per hour per pound thrust. The curves of specific fuel consumption are quite flat in the region of best-economy fuel flows and for maximum thrust operation at the flight speeds of 0, 190, 280, and 340 miles per hour

indicate fuel consumptions of 4.0, 3.8, 3.8, and 4.2 pounds of fuel per hour per pound of thrust, respectively. These values represent an increase in fuel consumption above the best-economy values of about 5 percent for flight speeds of 0 and 190 miles per hour and about 15 percent for flight speeds of 280 and 340 miles per hour. Reference to figure 12 shows that the predicted flight thrusts obtained at the best-economy fuel-air ratios are 420, 610, 660, and 680 pounds at the flight speeds of 0, 190, 280, and 340 miles per hour, respectively.

The fuel consumed per thrust horsepower-hour is plotted in figure 14 against fuel-air ratio for flight speeds of 190, 280, and 340 miles per hour. The spread between the different airspeed curves is due mainly to the reduction in jet-wake losses and the resultant increase in over-all operating efficiency obtained with increase in flight speed. The minimum values of power specific fuel consumption indicated in figure 14 are 6.9, 4.3, and 3.9 pounds per thrust horsepower-hour for the flight speeds of 190, 280, and 340 miles per hour, respectively. The best value of power specific fuel consumption (3.9 lb/thp-hr) corresponds to an over-all efficiency of 3.5 percent, as based on the lower heating value of the fuel; this efficiency value is about half that calculated for the idealized cycle.

Cycle pressures. - The cycling frequencies measured in the tests are given in tables I and II. A tabulation of the maximum and minimum combustion-chamber pressures is included in table II. The frequency values are seen to vary from 39 to 41 cycles per second. The maximum and minimum pressures were measured only in the tests conducted with the second flapper-valve assembly because the first tests were devoted to development of a satisfactory pickup. Table II shows that the maximum pressure increases from about 43 to about 52 inches of mercury gage (about 29 to 32 lb/sq in. absolute) when the simulated ram pressure is increased from 40 to 58 inches of water; those values compare with a theoretical maximum-pressure value of about 145 pounds per square inch absolute, which would be obtained in a constant-volume burning process. The minimum pressure is shown in table II to vary in a random manner from 7.5 to 10 inches of mercury vacuum (from 12.1 to 11.3 lb/sq in. absolute) for simulated ram pressures of 40 and 58 inches of water.

Photographic records of the combustion-chamber pressure variations as indicated on the oscilloscope screen are presented in figure 15 for two typical operating conditions. The small irregularities in the wave forms are due to the effects of the oscillating air column within the extension-tube connection to the pickup. The measured values of maximum and minimum combustion-chamber pressures

and of cycle time are identified on the individual pressure traces; the atmospheric and ram-pressure lines are estimated from linear interpolation between the maximum- and minimum-pressure values. The records show that the pressure rise from minimum to maximum value begins at a relatively slow rate and continues at substantially the same rate until a pressure somewhat higher than the absolute ram pressure is reached. At this pressure value, a high acceleration of pressure is obtained and the pressure then increases at a greatly increased rate to almost maximum value. The pressure decrease from maximum to minimum value occurs at a substantially constant rate. Values of the maximum rate of pressure rise and the rate of decrease for conditions (a) and (b) of figure 15 are roughly estimated from the records and are tabulated as follows:

Condition	Rate of pressure rise (in. Hg/sec)	Rate of pressure decrease (in. Hg/sec)
(a)	5,000	6000
(b)	13,000	4000

Flame photographs. - In figure 16, enlargements are shown of 14 successive frames of a high-speed motion-picture film of the flame at the tail-pipe outlet. A fluorescent tube lighted by standard 110-volt 60-cycle current provided a timing trace for the flame as shown in the enlargements. The frames show the distinct build-up and decay of the flame. Projection of the film clearly showed that the high-velocity discharge from the tail pipe was followed by a complete reversal of flow wherein a portion of the exhaust gases within the tail pipe and the nozzle was drawn back into the combustion chamber. This reversal of flow is the response to the suction pressures created within the combustion chamber after each explosion and probably results in precompression of the new charge and subsequent ignition.

Fuel-nozzle pressures. - The values of fuel-nozzle pressure measured in the tests on the first flapper-valve assembly were unduly high because of partial clogging of the nozzle passages by foreign materials within the fuel lines. These values are therefore not presented. The values measured for the second flapper-valve assembly are, however, considered satisfactory and are included in table II.

In figure 17, the fuel flow is plotted against the fuel-nozzle pressure (relative to atmospheric pressure) as measured in the tests on the second flapper-valve assembly. The values obtained in the fuel-distribution tests (fig. 7) are included in the plot for comparison. In the fuel-distribution tests the fuel nozzles discharged

against atmospheric pressure, whereas during operation of the engine the nozzles discharged against a cyclically varying pressure whose average is above atmospheric; the fuel pressures required in the engine-performanace tests are therefore higher than those measured in the fuel-distribution tests.

Steady-flow pressure loss across flapper-valve assembly. - The steady-flow pressure-loss characteristics of the two flapper-valve grid assemblies used in the tests are plotted in figure 18. The pressure differential required to open the flapper valves at the start of the performance tests is shown to be about 14 inches of water. Inasmuch as the pressure drop would vary closely as the square of the air-weight flow for constant flapper-valve position, the linear variation obtained throughout the range of pressure drops tested indicates that the valves were still opening and had not reached wide-open position even at a pressure drop of 40 inches of water. In view of the fact that the two flapper-valve assemblies were similar the stiffness and natural frequency and hence the steady-flow pressure-loss characteristics would be the same as confirmed in figure 18.

Flapper-valve deterioration. - Figure 19 is a photograph of the first flapper-valve assembly taken after 30 minutes of operation. In general, most of the valves appeared to be in good condition. The discoloration of some of the valves indicated that they had been subjected to hot burning gases; as a consequence these valves had lost their original tension. Details of the two most damaged valves in the assembly are shown in figure 20. Sections of the tips of these two valves were broken off and cracks extended back from the edges. The damage was undoubtedly the result of impact forces imposed on the valves as no signs of discoloration were apparent. Further testing with this valve assembly (not reported herein) indicated a rapid reduction in thrust after 33 minutes of total operation.

Inspection of the second flapper-valve assembly after 17 minutes of operation revealed greater flapper-valve damage than that of the first assembly, notwithstanding the shorter operating time.

SUMMARY OF RESULTS

A summary of the important results obtained in sea-level tests conducted on a 22-inch-diameter pulse-jet engine installed on a thrust stand is presented in the following table:

Simulated ram pressure, in. water	0	18	40	58
Equivalent indicated airspeed (NACA air), mph	0	190	280	340
Predicted maximum flight thrust, lb	500	660	740	770
Thrust specific fuel consumption at maximum-thrust operation, lb/(hr)(lb thrust)	4.0	3.8	3.8	4.2
Predicted flight thrust for operation at minimum fuel consumption, lb	420	610	660	680
Minimum value of thrust specific fuel consumption, lb/(hr)(lb thrust)	3.8	3.4	3.3	3.6

Maximum-thrust operation was obtained at a fuel-air ratio of approximately 0.08 and best fuel economy, in the fuel-air-ratio range between 0.064 and 0.072.

The operating frequency of the jet engine varied from 39 to 41 cycles per second. Maximum combustion-chamber pressures in the order of 40 to 50 inches of mercury gage and minimum pressures from about 7 to 10 inches of mercury vacuum were measured for the simulated ram pressures of 40 and 58 inches of water. The operating lives of the two flapper-valve assemblies used in the tests were approximately 17 and 33 minutes, respectively.

Aircraft Engine Research Laboratory,
National Advisory Committee for Aeronautics,
Cleveland, Ohio, October 2, 1945.

TABLE I - SUMMARY OF RESULTS OF TESTS ON FIRST STANDARD FLAPPER-VALVE ASSEMBLY

Run	Simulated ram pressure (in. water)	Fuel flow (lb/hr)	Barometric pressure (in. Hg abs.)	Combustion-air temperature (°F)	Combustion-air weight flow, W (lb/hr)	Fuel-air ratio	Jet thrust $\frac{W}{g} V_j$ (lb)	Effective jet velocity, V_j (ft/sec)	Predicted flight thrust $\frac{W}{g}(V_j - V_o)$ (lb)	Cycling frequency (cps)	Maximum valve-grid temperature (°F)	Maximum shell temperature (°F)	Total time on flapper valve at end of run (min)
1	19.8	1600	29.42	59	[a]26,280	0.061	513	2262	447	------	104	1540	5.5
3	18.2	2000	29.26	68	[a]28,800	.069	640	2579	571	------	96	1220	-------
4	20.4	1600	29.26	71	[a]26,280	.061	457	2016	389	------	114	1600	8.0
5	17.1	2210	29.05	60	[a]29,880	.074	695	2697	625	40	94	1500	9.8
6	16.6	2400	29.05	64	[a]30,600	.078	744	2818	673	40	104	950	11.3
8	-0.5	2000	29.30	68	[a]25,200	.079	496	2279	496	39	103	1175	-------
9	- .1	1600	29.30	70	[a]21,600	.074	427	2292	427	39	118	1550	14.1
12	15.9	2400	28.95	78	[a]30,600	.078	711	2693	640	40	112	1200	-------
14	17.5	2000	28.95	76	[a]28,800	.069	579	2330	509	40	112	1150	18.1
15	0.1	2200	29.50	64	[a]25,560	.086	487	2210	487	40	-------	950	18.9
16	2.0	1400	29.50	65	-------	-----	----	------	----------	40	87	1050	20.2
18	37.7	2800	29.35	63	[a]36,000	.078	870	2801	748	39	105	1200	-------
19	41.5	2400	29.35	65	[a]34,200	.070	794	2691	672	40	96	1585	21.7
20	40.2	2000	29.35	64	[a]32,040	.062	691	2498	579	40	100	1100	-------
21	40.9	1800	29.35	71	[a]30,960	.058	543	2030	433	41	103	1415	23.4
22	40.7	3200	29.35	64	[a]37,440	.085	815	2525	683	------	104	1150	24.3
23	20.4	1600	29.18	60	26,280	.061	----	------	----------	------	-------	-------	-------
24	18.4	2000	29.18	63	29,160	.069	[b]655	2602	584	------	-------	-------	-------
25	20.5	2200	29.18	66	29,520	.075	----	------	----------	------	-------	-------	-------
26	17.3	2400	29.18	67	30,600	.078	742	2812	670	------	-------	-------	26.5
27	-0.2	1600	29.18	62	21,600	.074	[b]403	2165	403	------	-------	-------	-------
28	-2.4	1800	29.18	65	24,120	.075	[b]470	2261	470	------	-------	-------	-------
29	-2.1	2000	29.18	68	25,200	.079	514	2364	514	------	-------	-------	28.2
30	43.3	2000	29.18	74	34,920	.057	[b]758	2515	629	------	-------	-------	-------
31	42.0	2400	29.18	74	34,560	.069	[b]840	2818	715	------	-------	-------	-------
32	38.0	2800	29.18	75	34,920	.080	859	2854	739	------	-------	-------	29.9
33	60.4	2400	29.42	80	37,440	.064	818	2531	659	------	104	1250	-------
34	59.3	2200	29.42	84	38,880	.057	729	2177	566	------	-------	-------	31.6
35	61.5	2800	29.42	89	38,880	.072	907	2707	739	------	127	1250	-------
36	59.5	3200	29.42	91	39,600	.081	933	2729	765	------	127	-------	33.3

[a]Read from plot of data obtained in runs 23 to 32.

[b]Stabilization time for thrust measurement less than 30 sec.

TABLE II - SUMMARY OF RESULTS OF TESTS ON SECOND STANDARD FLAPPER-VALVE ASSEMBLY

Run	Simulated ram pressure (in. water)	Fuel flow (lb/hr)	Fuel-nozzle pressure (lb/sq in.)	Barometric pressure (in. Hg absolute)	Combustion-air temperature (°F)	Combustion-air weight flow W (lb/hr)	Fuel-air ratio	Jet thrust $\frac{W}{g} V_j$ (lb)	Effective jet velocity V_j (ft/sec)
2	59.0	3200	62	28.94	85	41,040	0.078	946	2674
3	60.1	2500	38	28.94	86	38,880	.064	884	2638
4	58.7	3500	72	28.94	85	41,760	.084	973	2702
5	58.1	2800	48	28.94	85	39,600	.071	883	2583
9	55.8	2800	48	29.08	70	39,600	.071	------	------
10	53.8	2800	48	29.08	72	40,680	.069	892	2540
15	59.0	2800	------	28.98	78	42,100	.067	923	2541
16	36.7	2800	47	28.99	69	37,080	.076	829	2591
17	39.9	2000	27	28.99	70	32,040	.062	731	2644
18	37.5	3000	55	28.99	72	37,080	.081	875	2735
19	35.9	2400	37	28.99	72	33,480	.072	810	2804

Run	Predicted flight thrust $\frac{W}{g} (V_j - V_o)$ (lb)	Cycling frequency (cps)	Maximum combustion pressure (in. Hg gage)	Minimum combustion pressure (in. Hg vacuum)	Maximum valve-grid temperature (°F)	Maximum shell temperature (°F)	Total time on flapper valve at end of run (min)
2	772	39	47.6	9.5	134	1375	--------
3	717	40	47.6	8.5	136	-------	3.0
4	795	-------	51.6	9.2	120	1325	--------
5	716	-------	51.1	8.0	126	1550	4.8
9	----------	40	52.4	8.6	148	1700	8.3
10	727	39	52.4	9.2	150	1225	9.2
15	745	-------	----------	--------	------	-------	13.6
16	703	39	----------	10.0	153	1300	--------
17	618	40	43.4	7.4	162	1600	15.7
18	747	38	45.3	10.2	151	1200	--------
19	697	40	41.9	8.4	151	1575	17.3

National Advisory Committee for Aeronautics

E-269

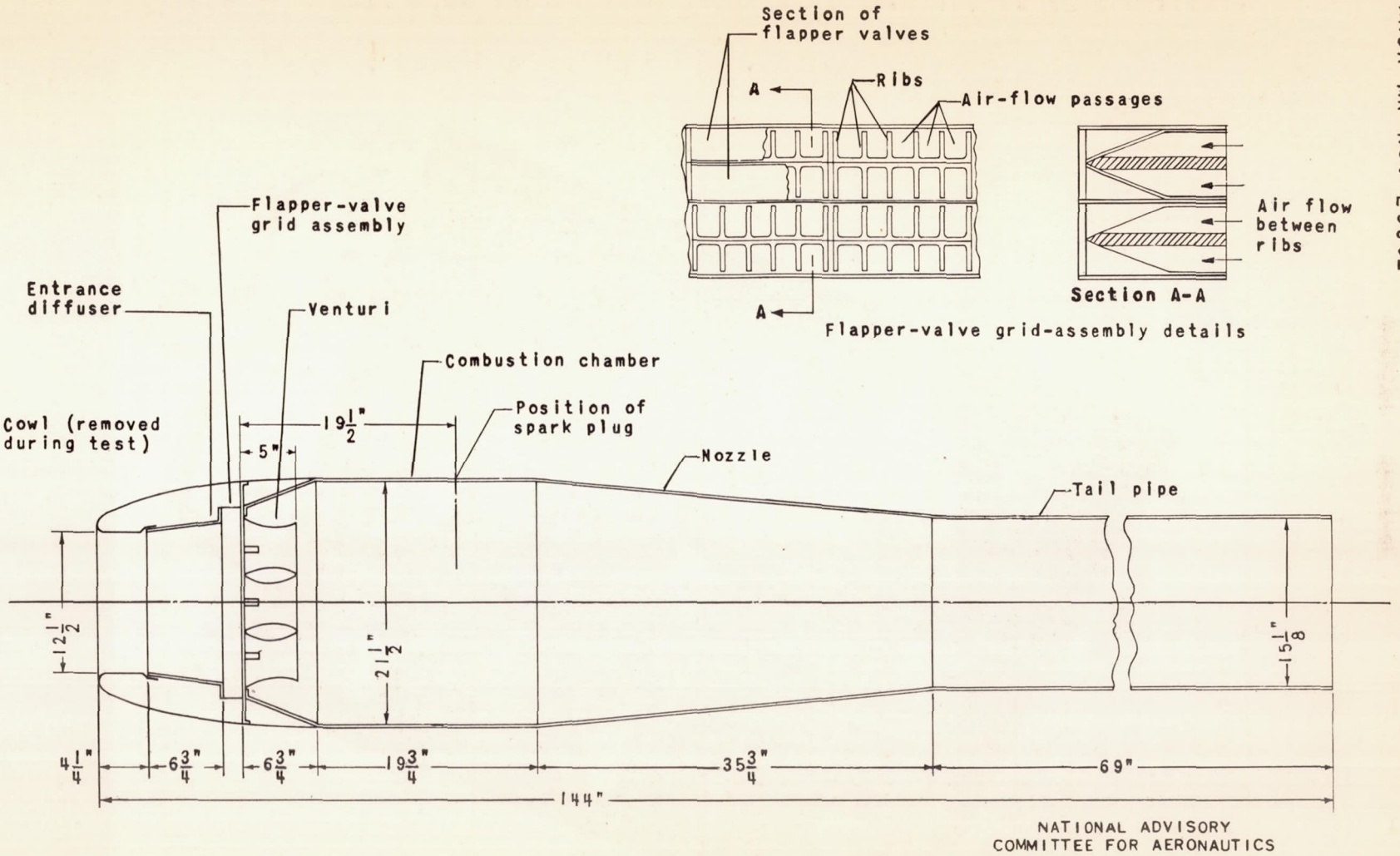

Figure 1. - Details of 22-inch-diameter pulse-jet engine.

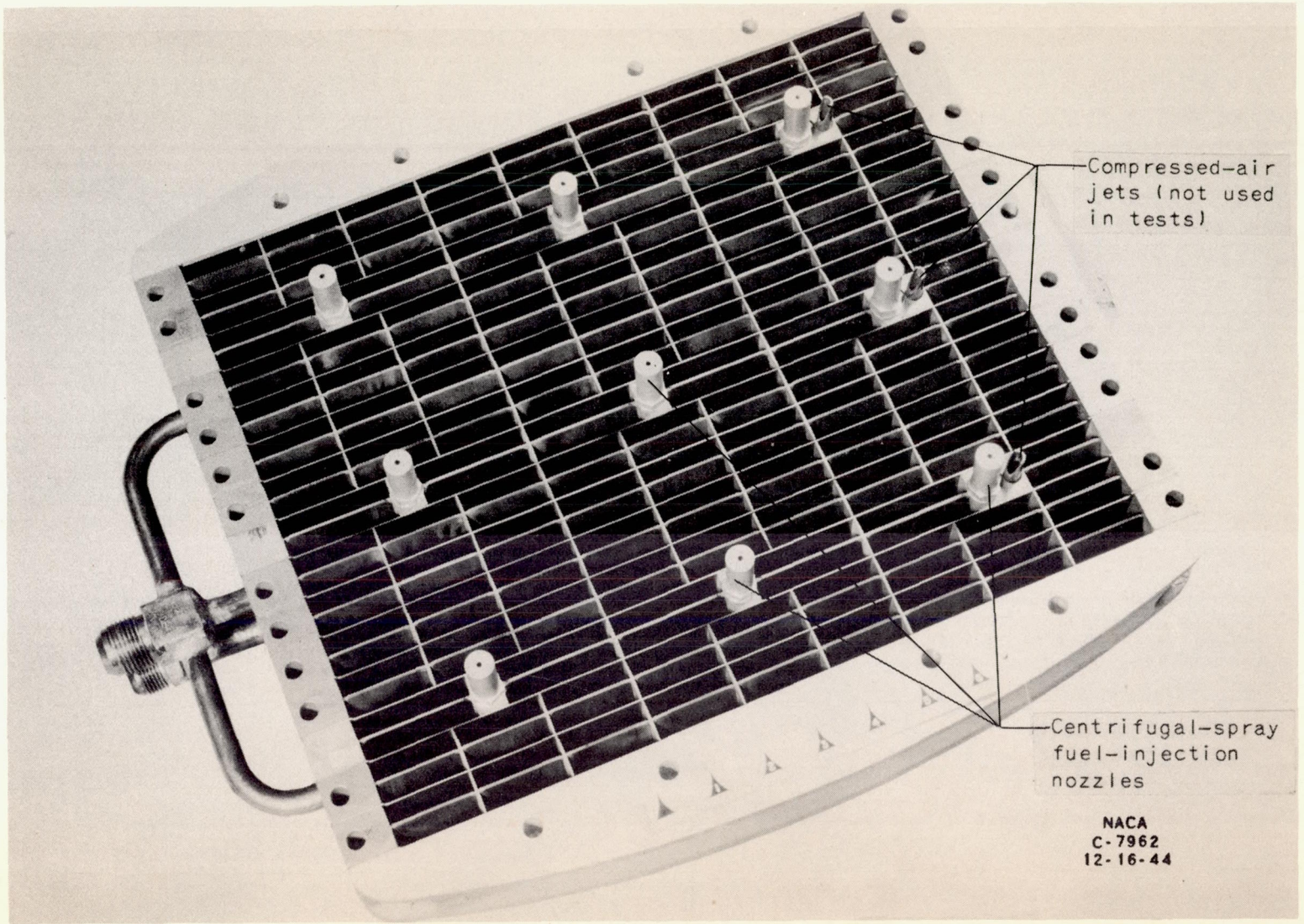

Figure 2. - Rear view (downstream face) of flapper-valve grid assembly.

NACA MR No. E5J02

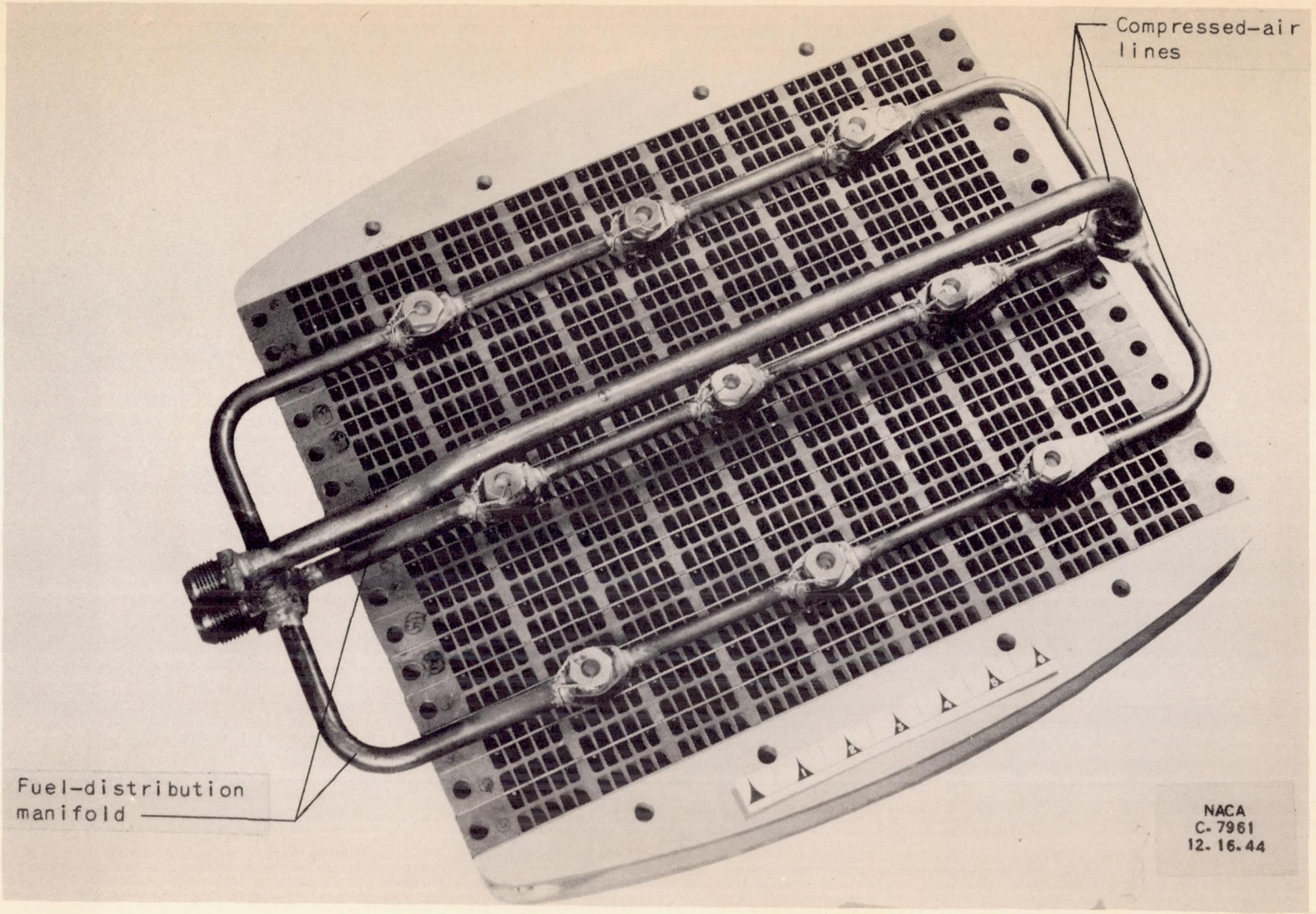

Figure 3. - Front view (upstream face) of flapper-valve grid assembly.

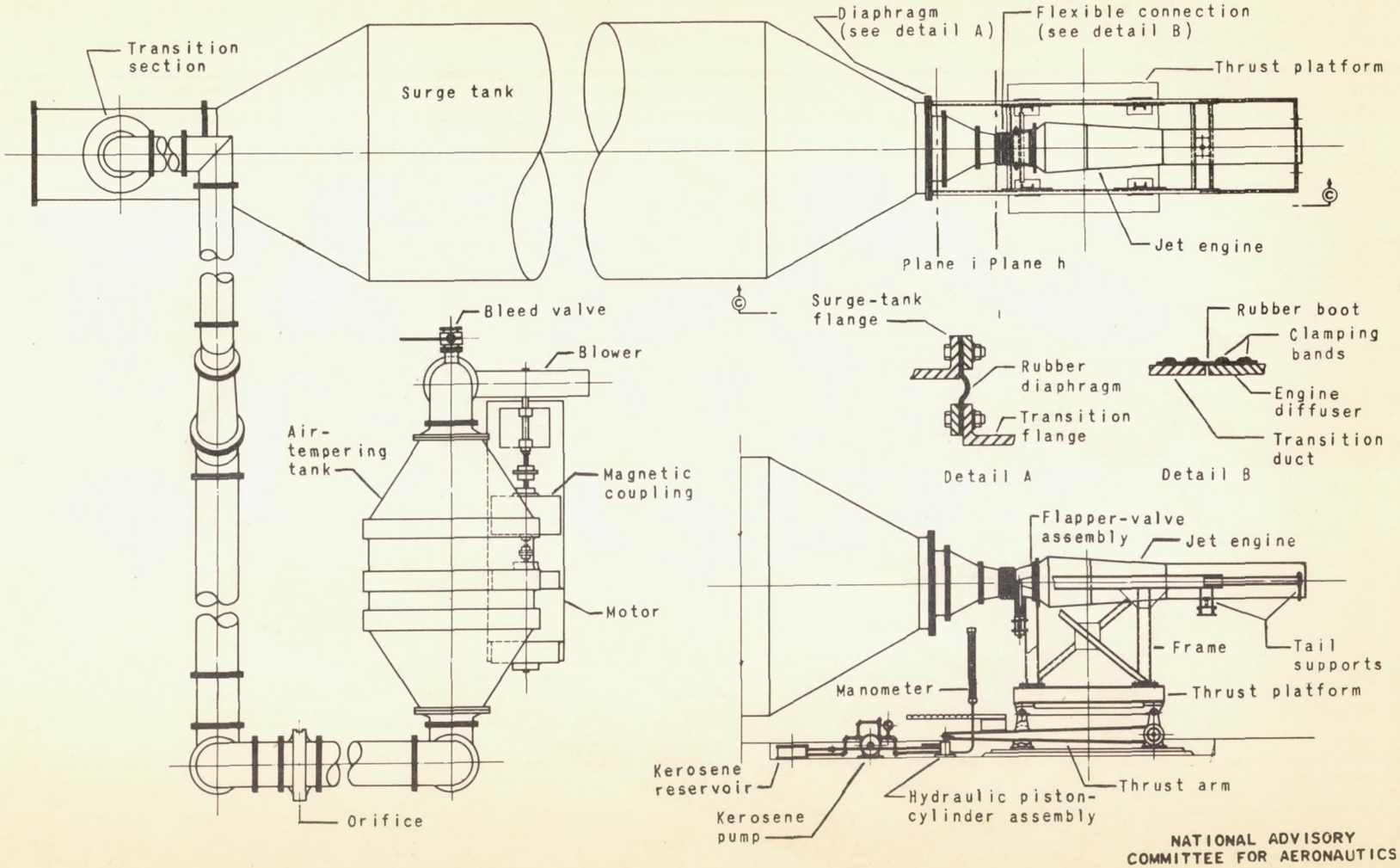

Figure 4. - Schematic diagram of test installation of 22-inch-diameter pulse-jet engine.

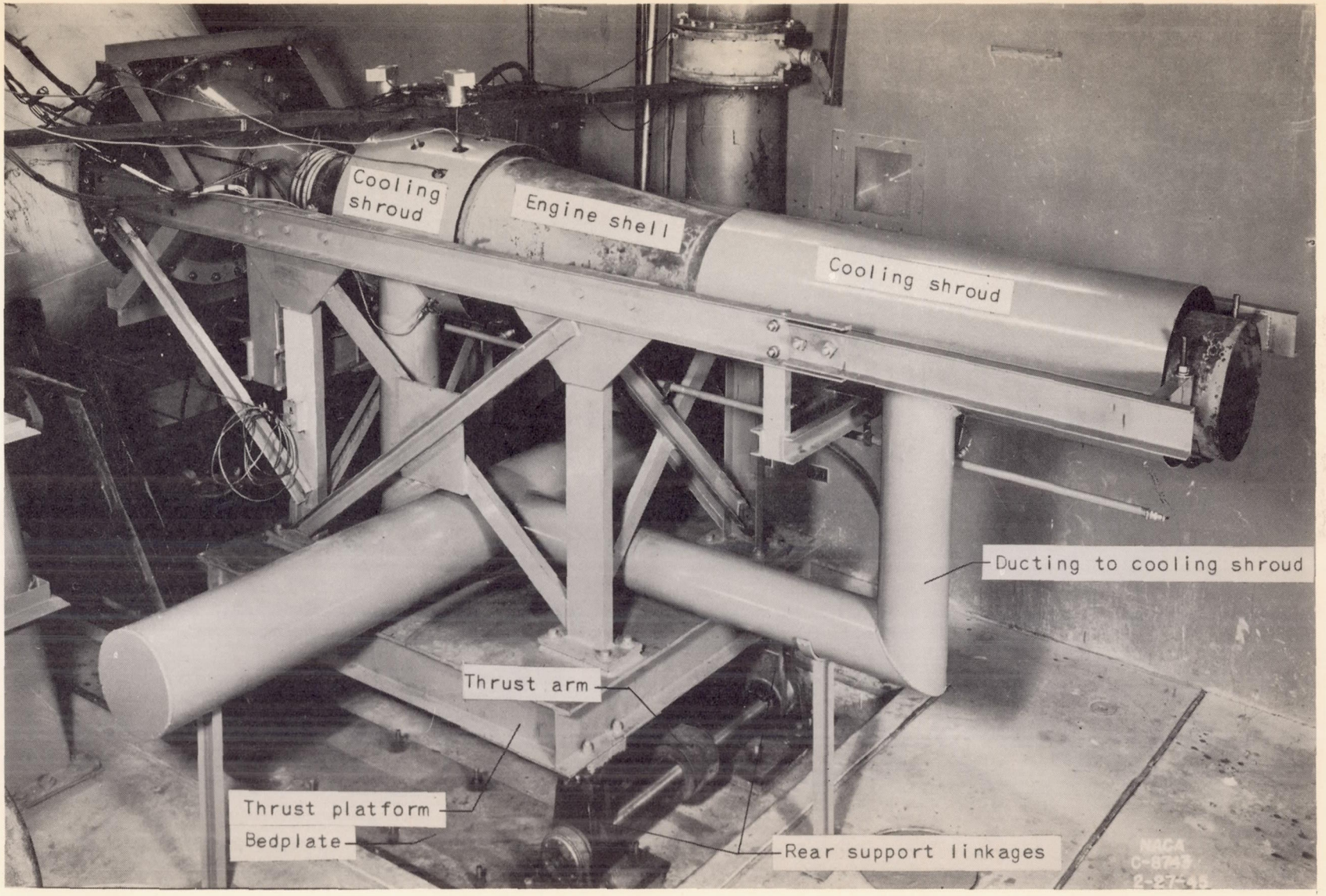

Figure 5. - Test installation of 22-inch-diameter pulse-jet engine.

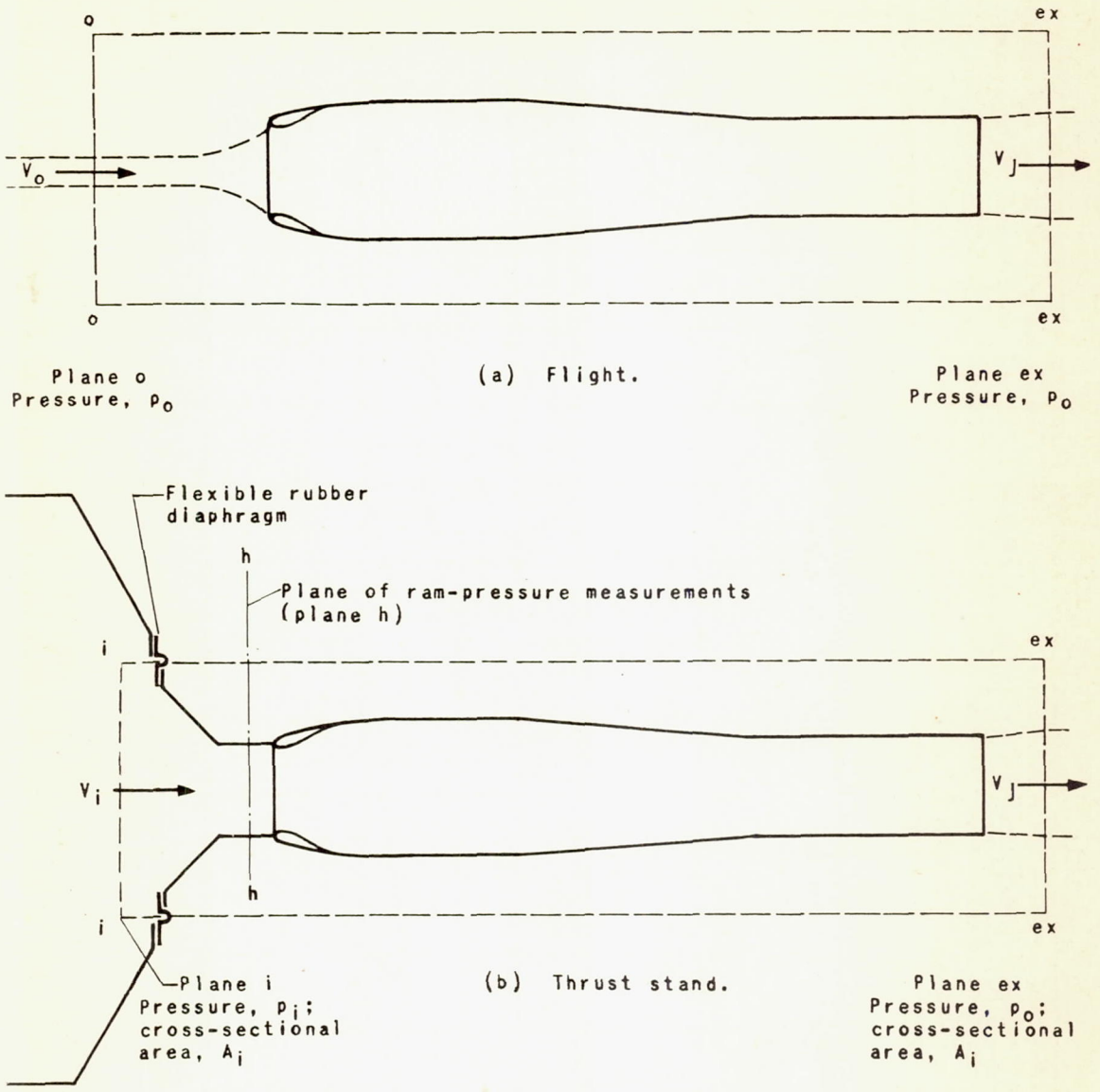

Figure 6. - Comparison of flow conditions obtained in thrust-stand tests with those existing in flight.

E-269

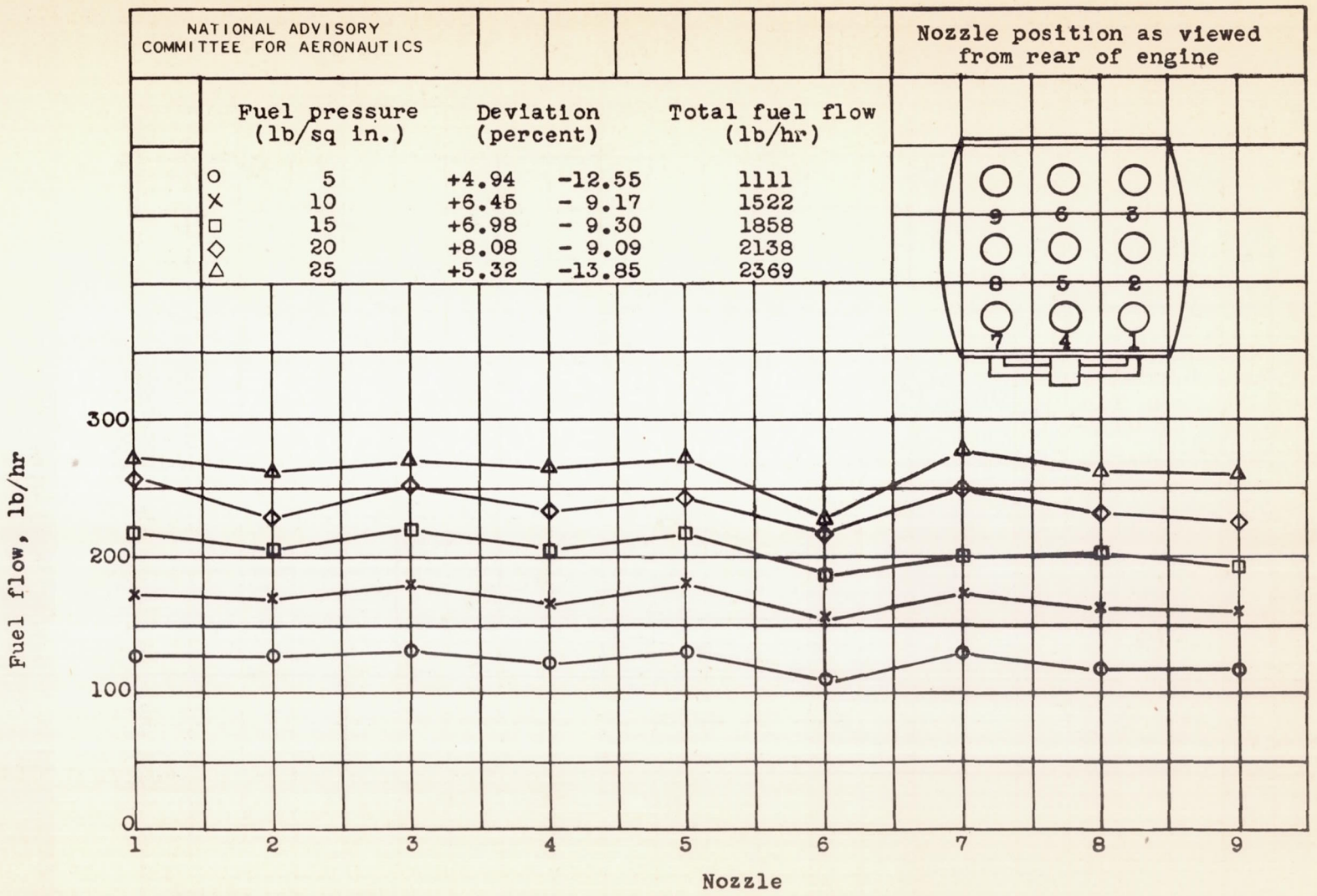

Figure 7.- Results of flow-bench tests on fuel-injection nozzles showing individual-nozzle fuel flows.

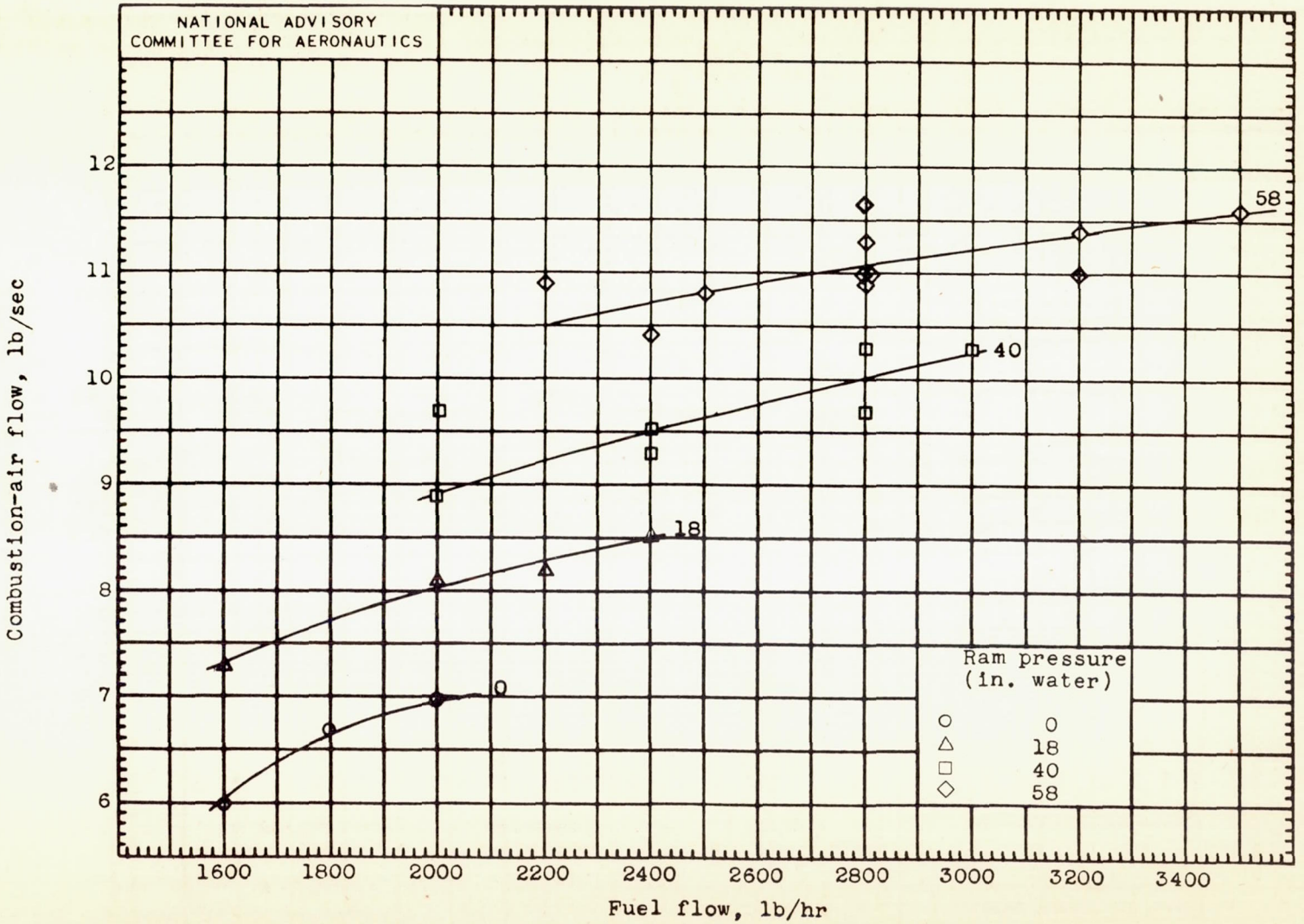

Figure 8.- Variation of combustion-air weight flow with fuel flow for the test simulated ram pressures.

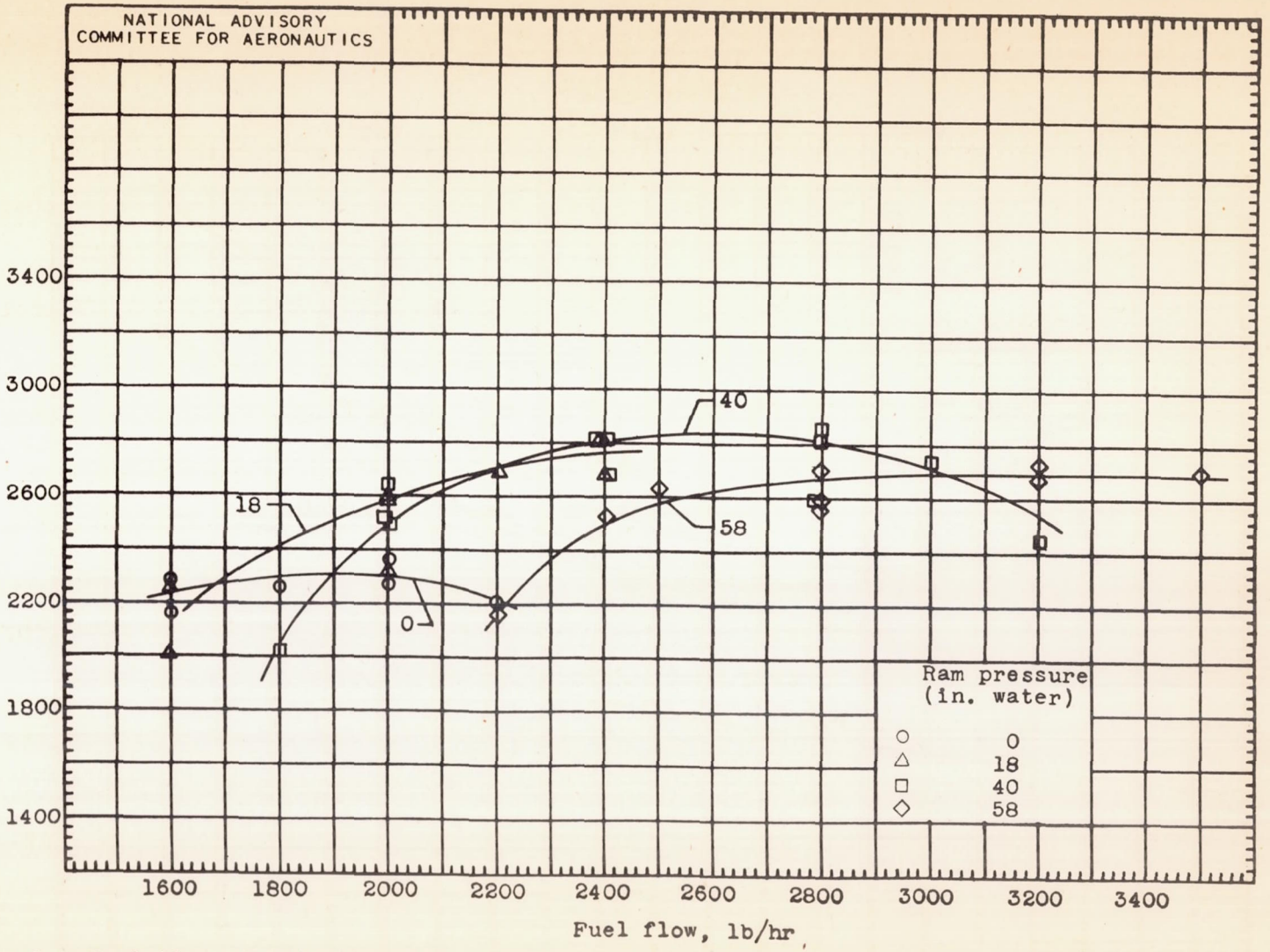

Figure 9.- Variation of effective jet velocity with fuel flow for the test simulated ram pressures.

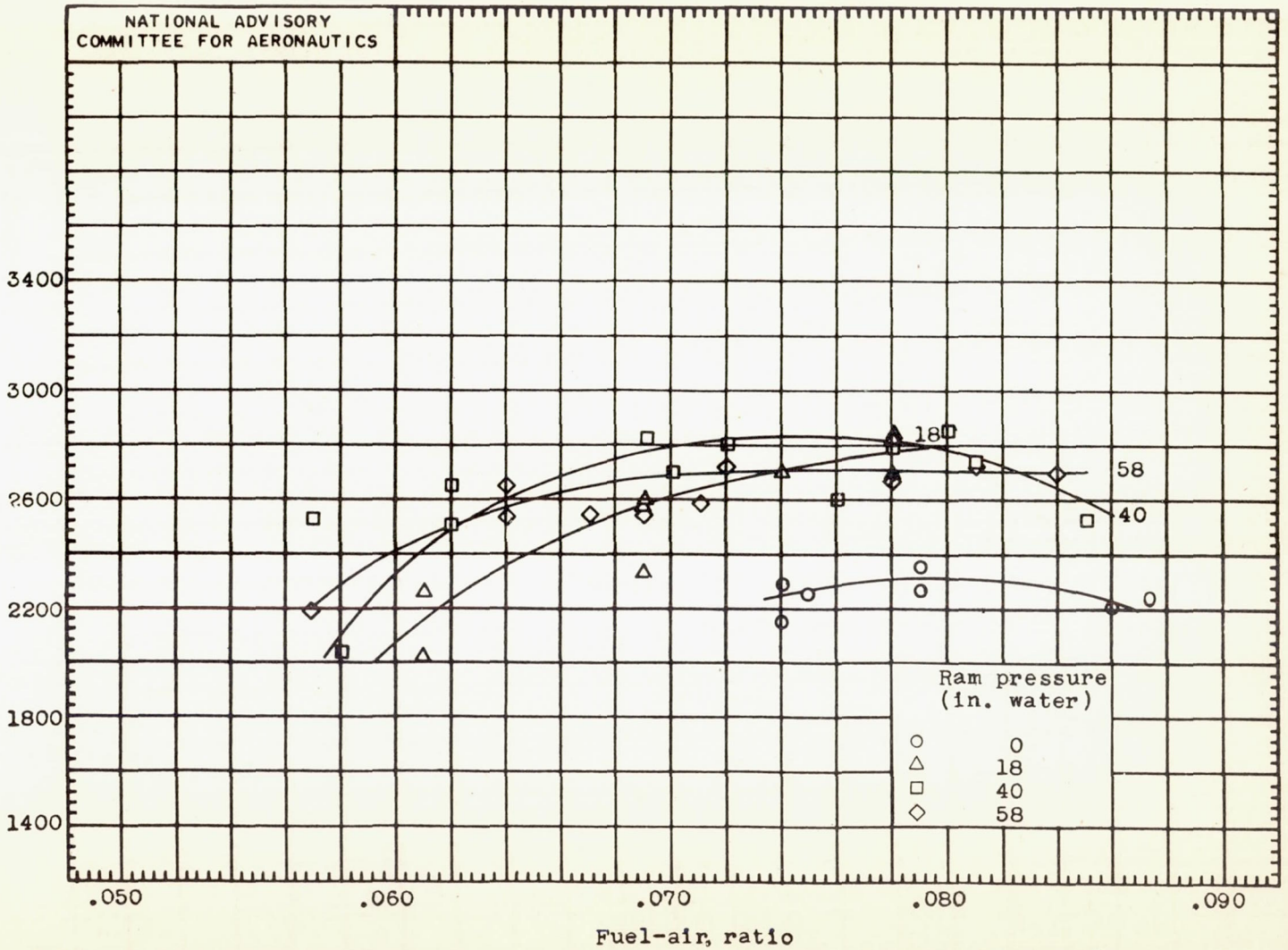

Figure 10.-Variation of effective jet velocity with fuel-air ratio for the test simulated ram pressures.

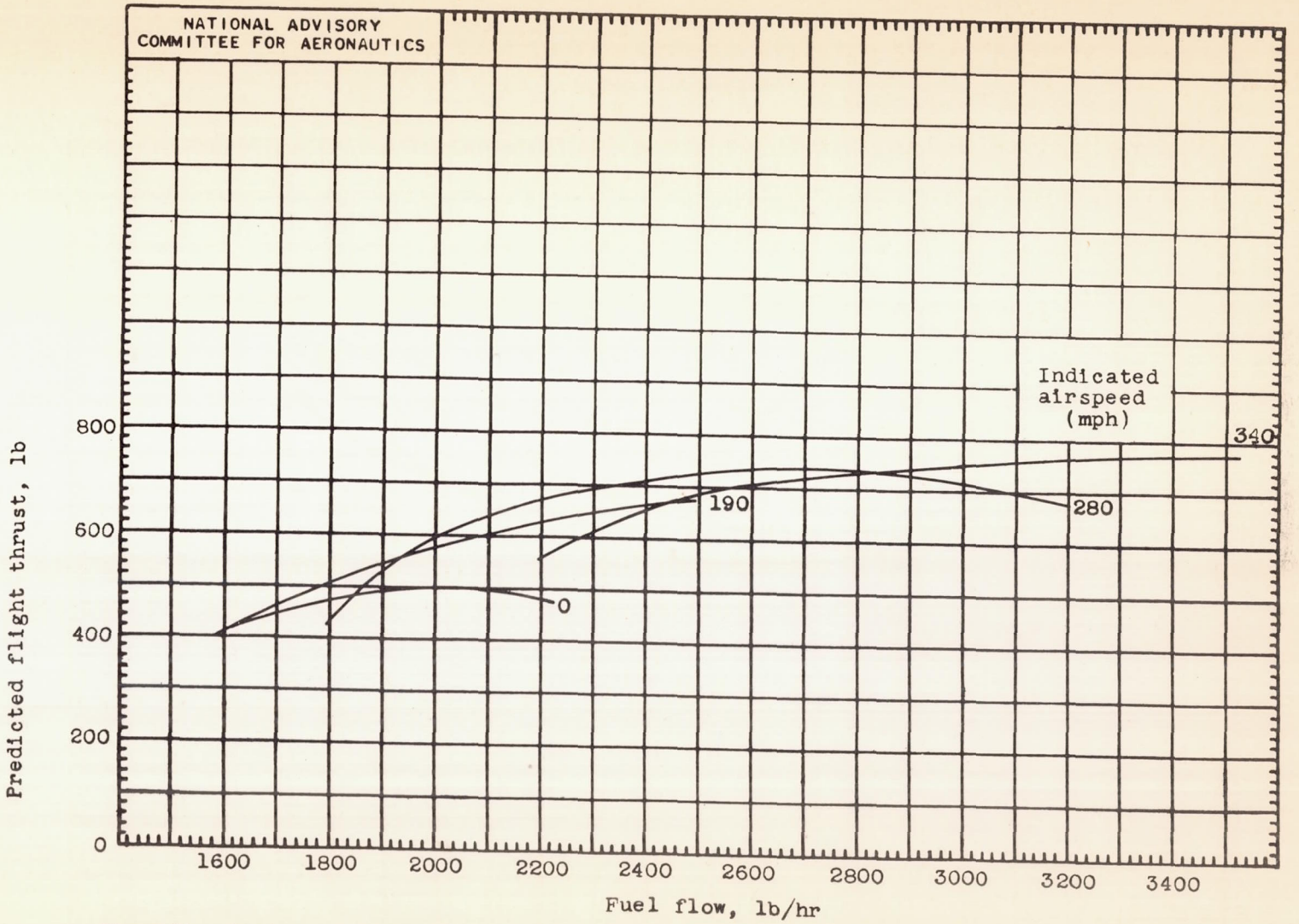

Figure 11. - Variation of predicted flight thrust (excluding external drag) with fuel flow for the various simulated flight speeds. (Sea-level operation in approximately NACA air.)

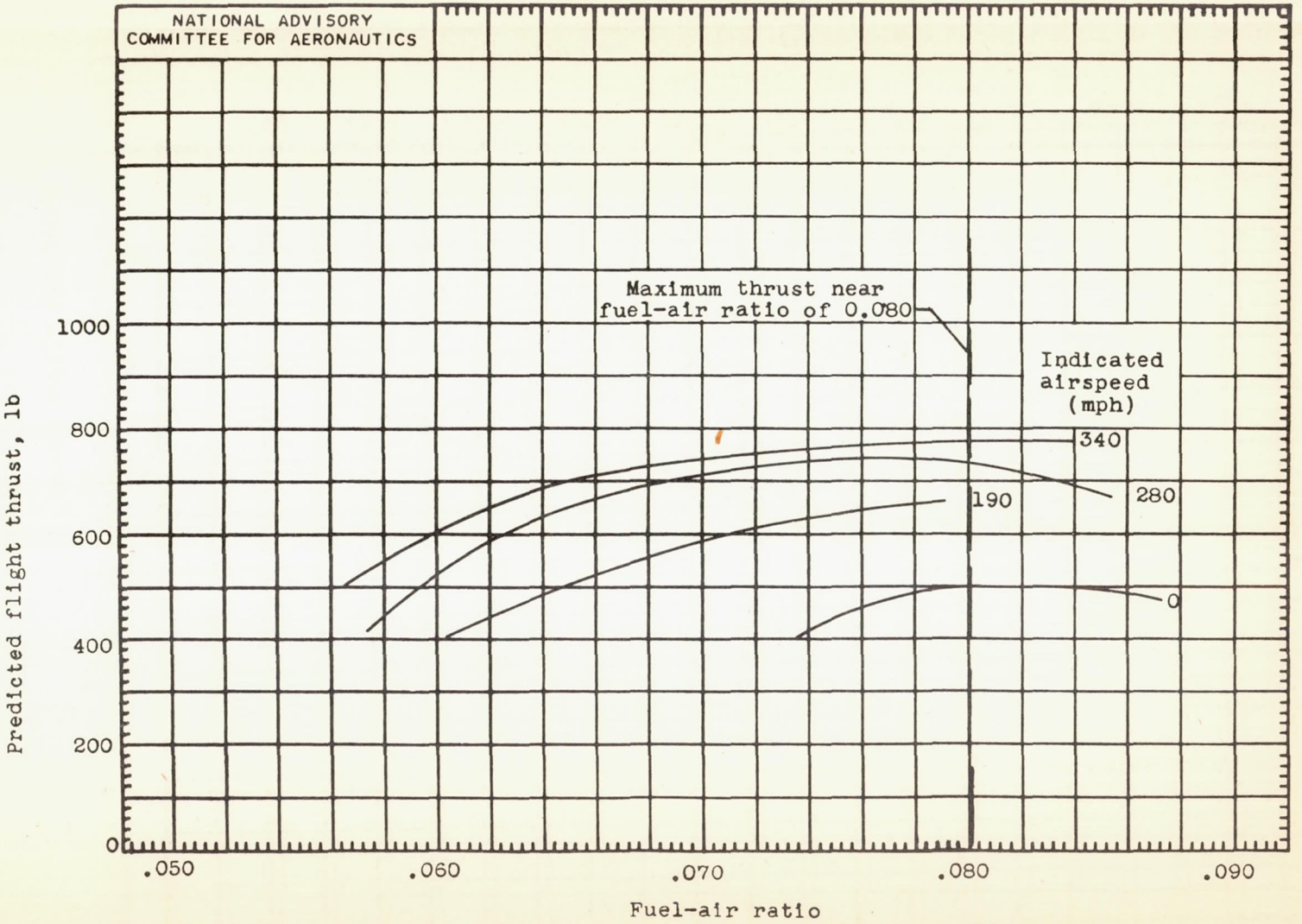

Figure 12. - Variation of predicted flight thrust (excluding external drag) with fuel-air ratio for the various simulated flight speeds. (Sea-level operation in approximately NACA air.)

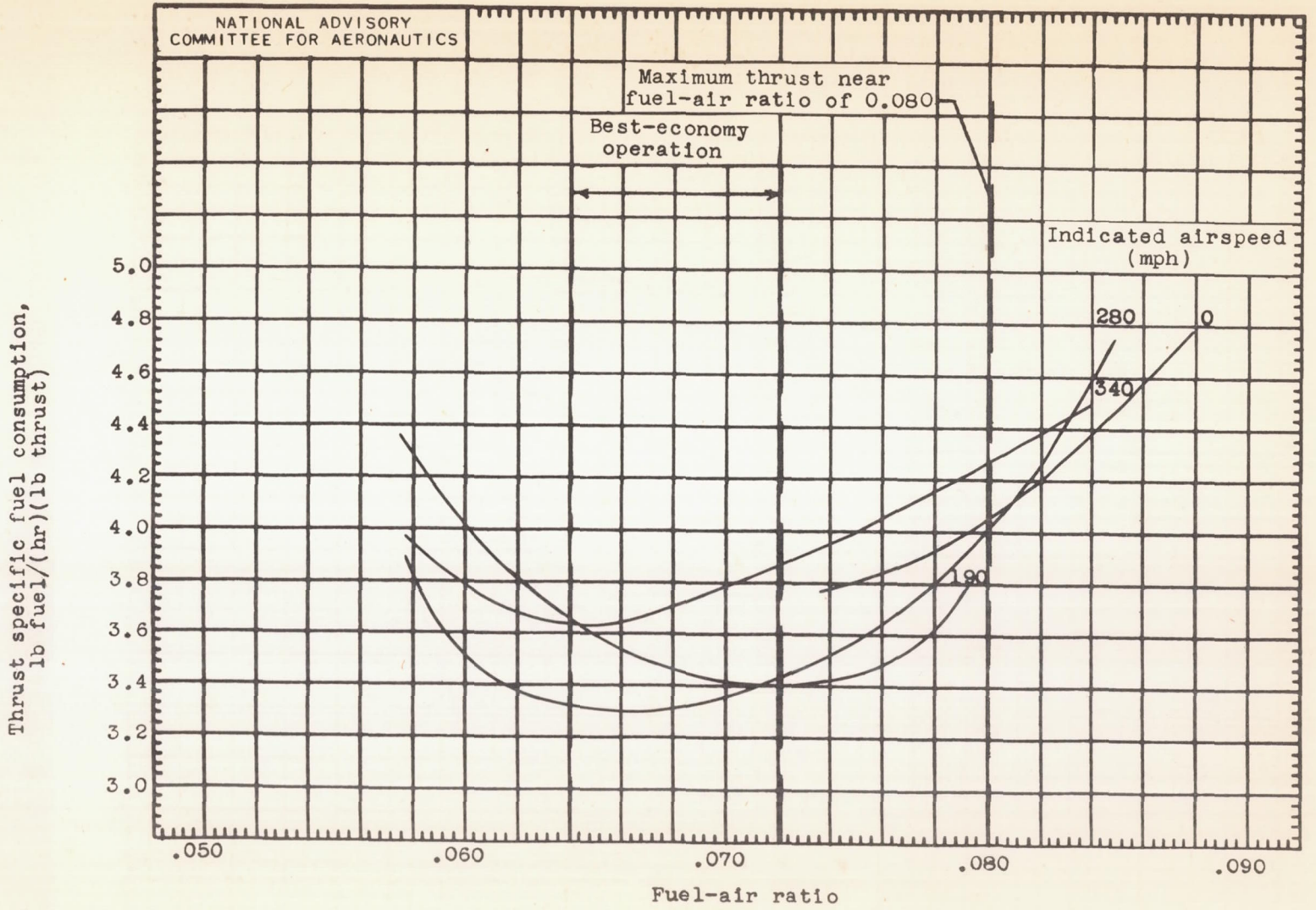

Figure 13.- Variation of thrust specific fuel consumption with fuel-air ratio for the various simulated flight speeds. (Sea-level operation in approximately NACA air.)

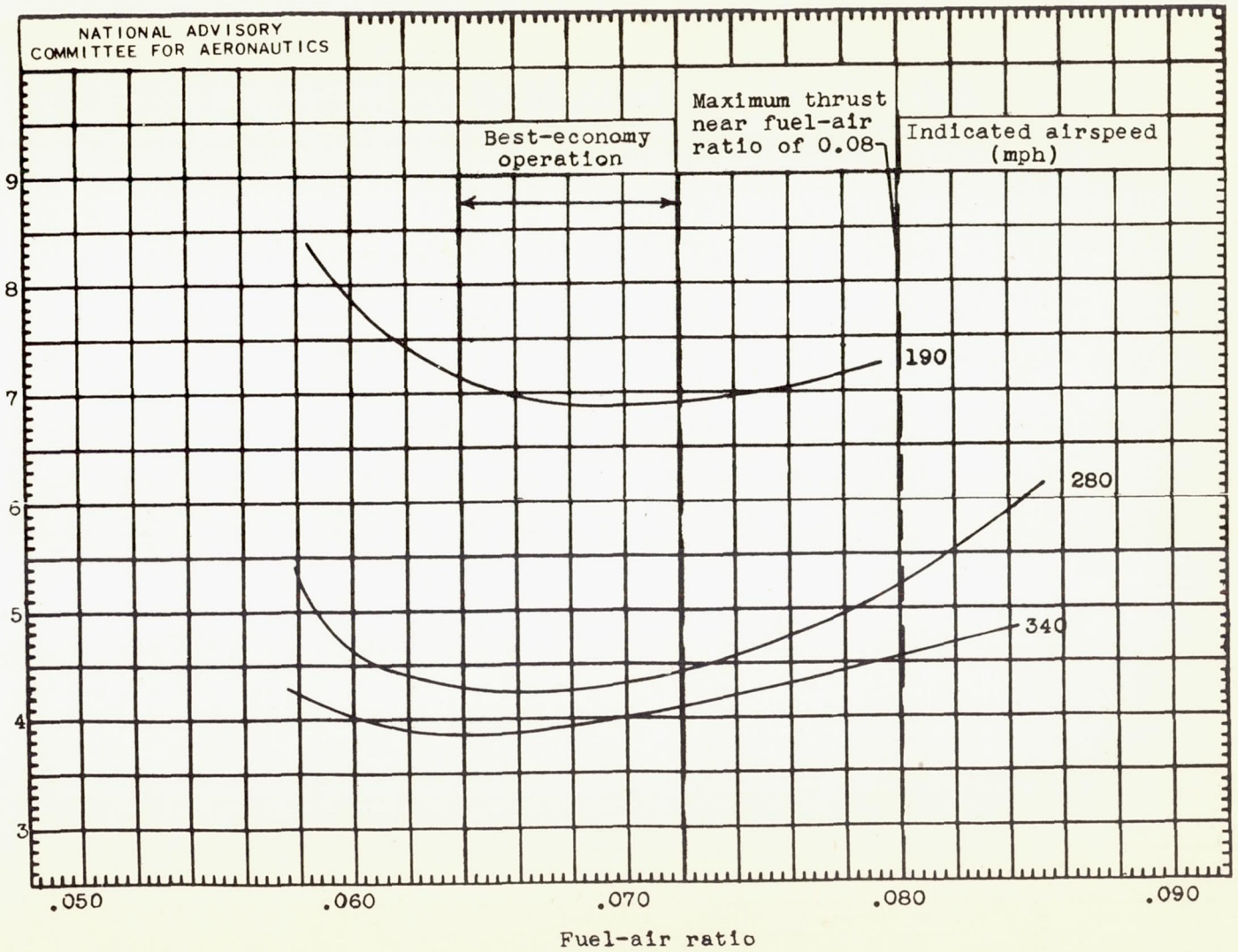

Figure 14. - Variation of power specific fuel consumption with fuel-air ratio for the various simulated flight speeds. (Sea-level operation in approximately NACA air.)

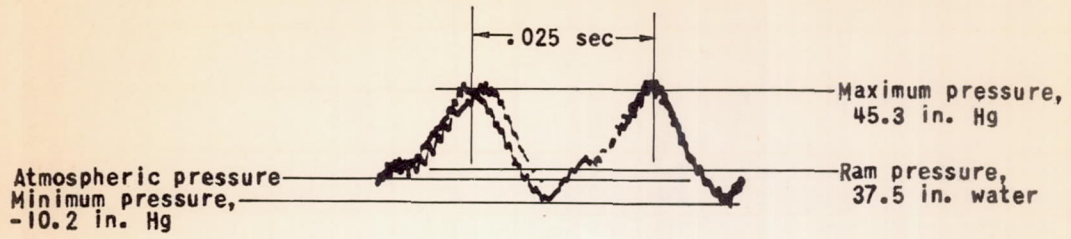

(a) Ram pressure, 37.5 inches of water; fuel flow, 3000 pounds per hour; fuel-air ratio, 0.081.

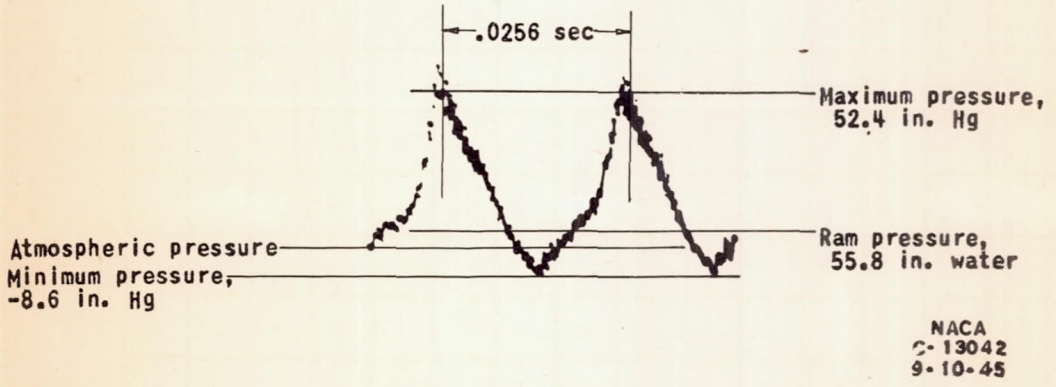

(b) Ram pressure, 55.8 inches of water; fuel flow, 2800 pounds per hour; fuel-air ratio, 0.071.

Figure 15. - Combustion-chamber pressure cycles for two typical test conditions.

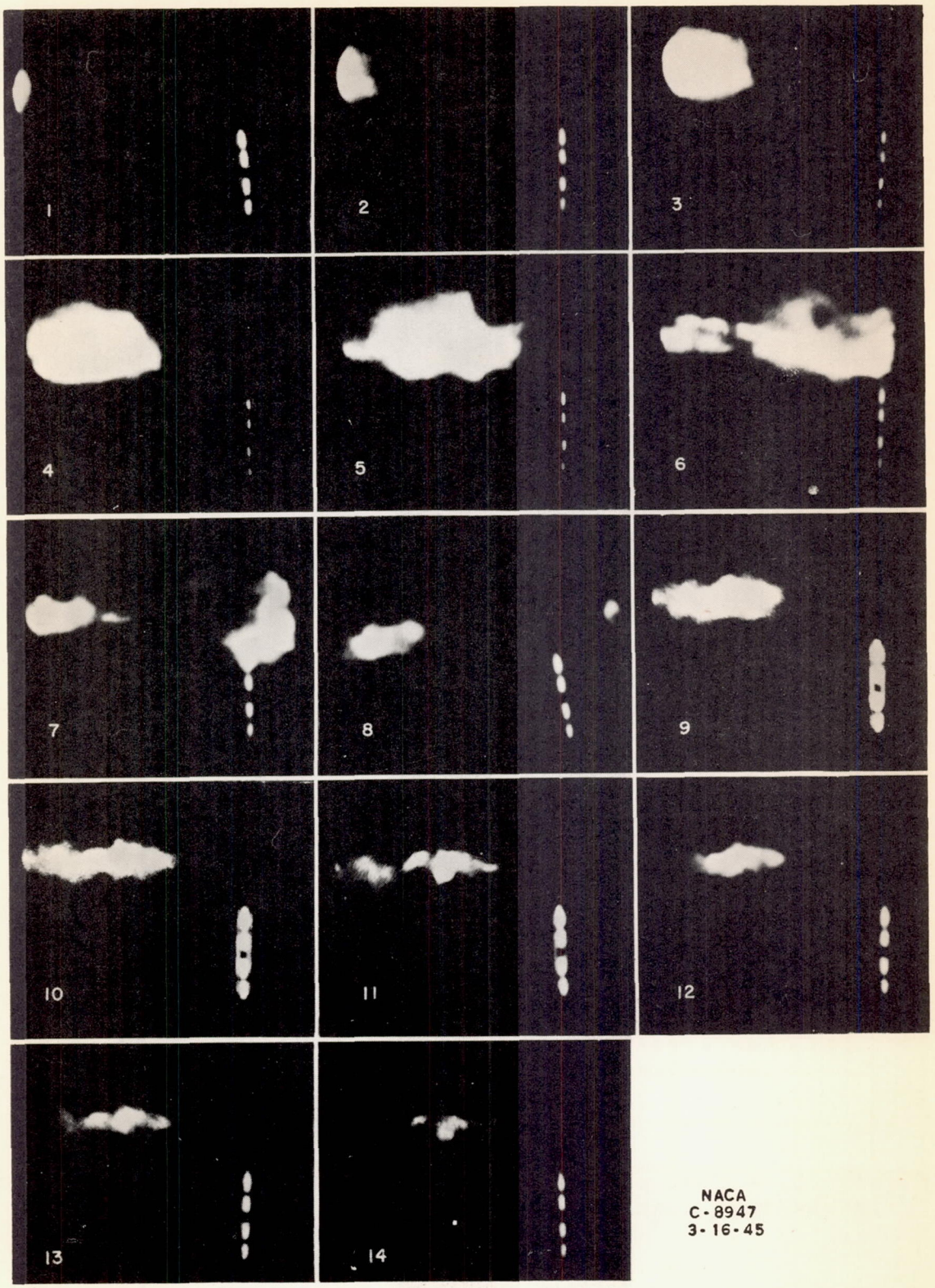

Figure 16. - The flame cycle at the tail-pipe outlet as viewed by a high-speed motion-picture camera (2000 frames per sec).

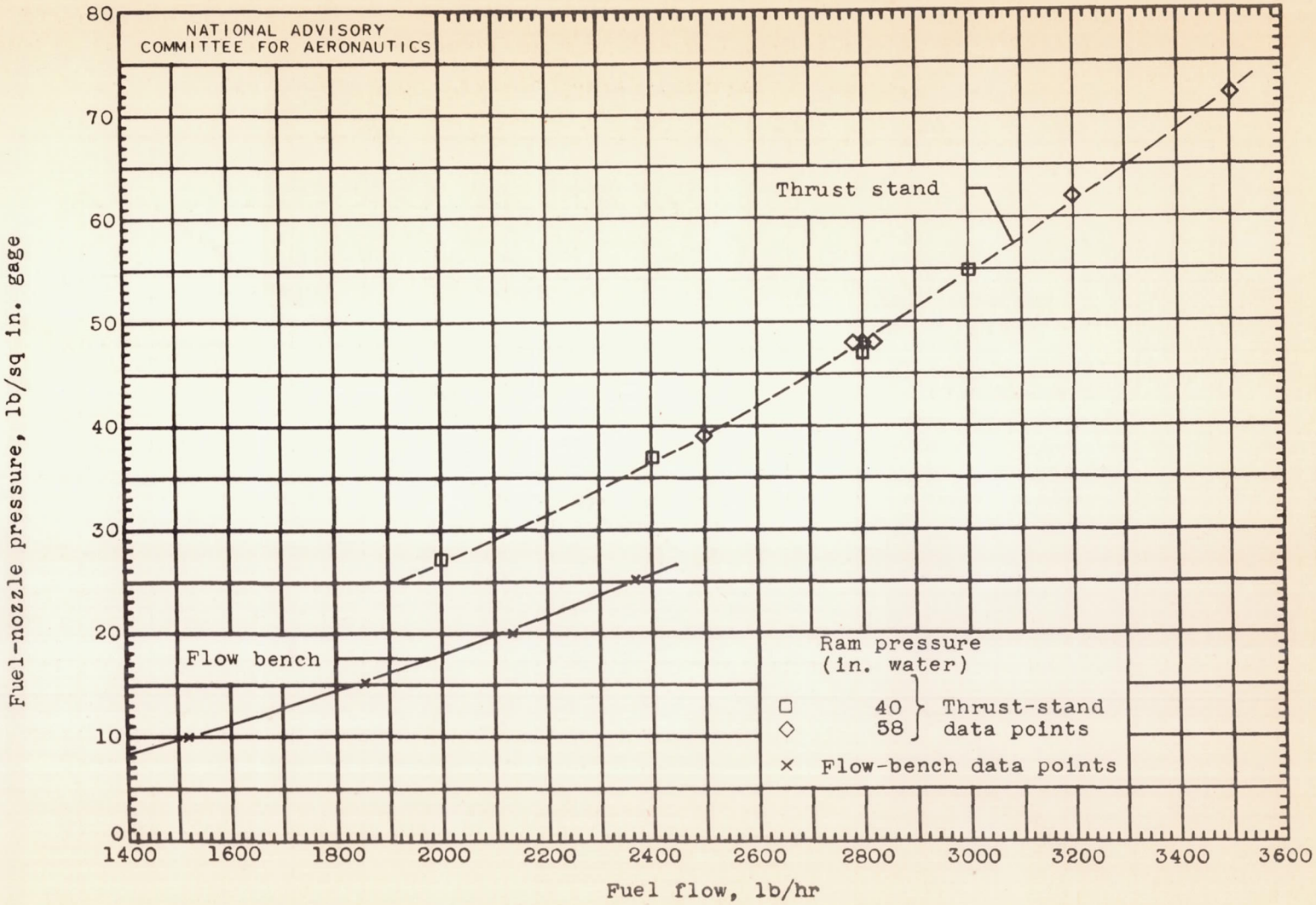

Figure 17.- Variation of fuel-nozzle pressure with fuel flow showing difference of thrust-stand data (obtained during operation) from the flow-bench calibration.

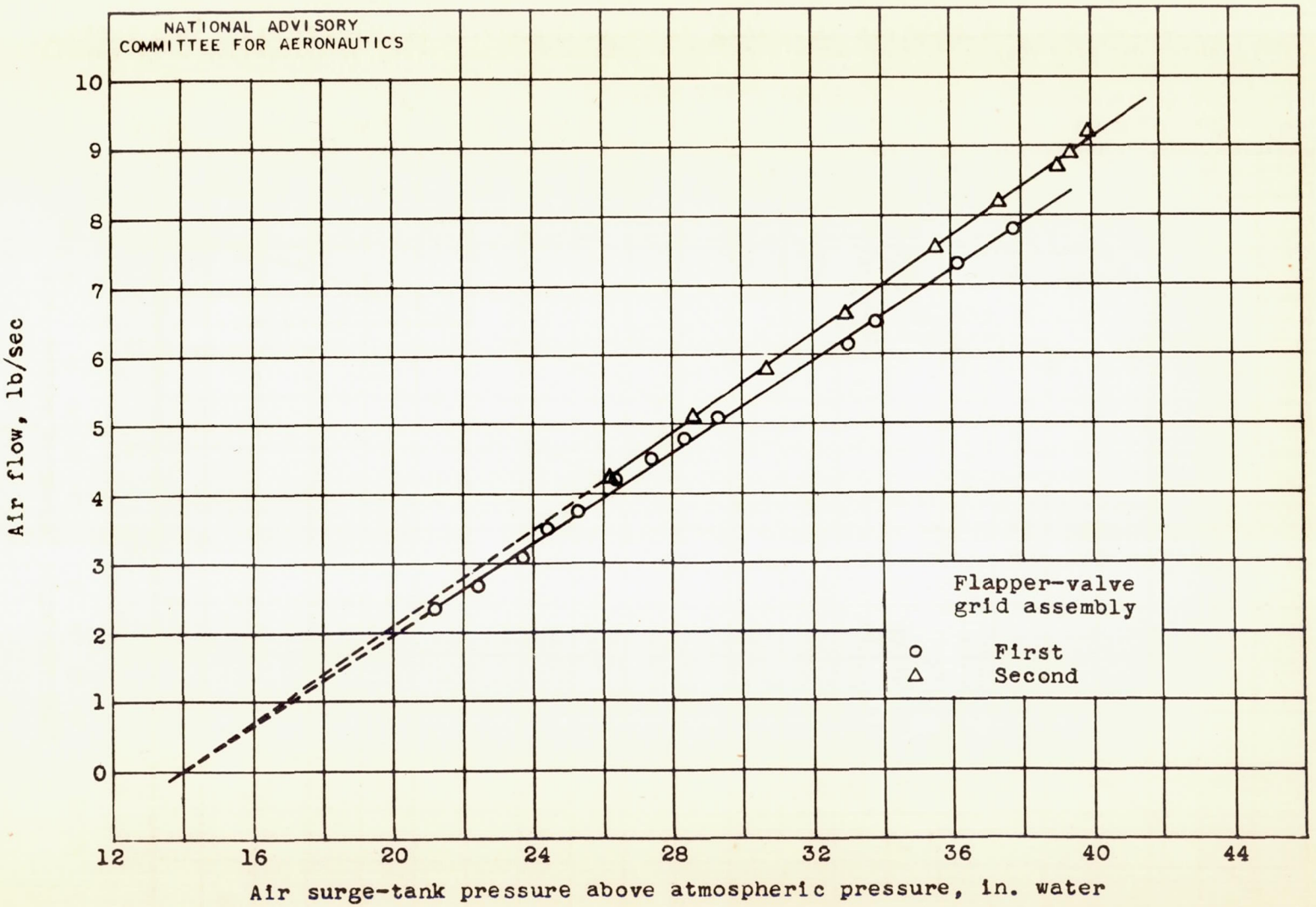

Figure 18.- Pressure-loss characteristics of the two flapper-valve grid assemblies in the performance tests.

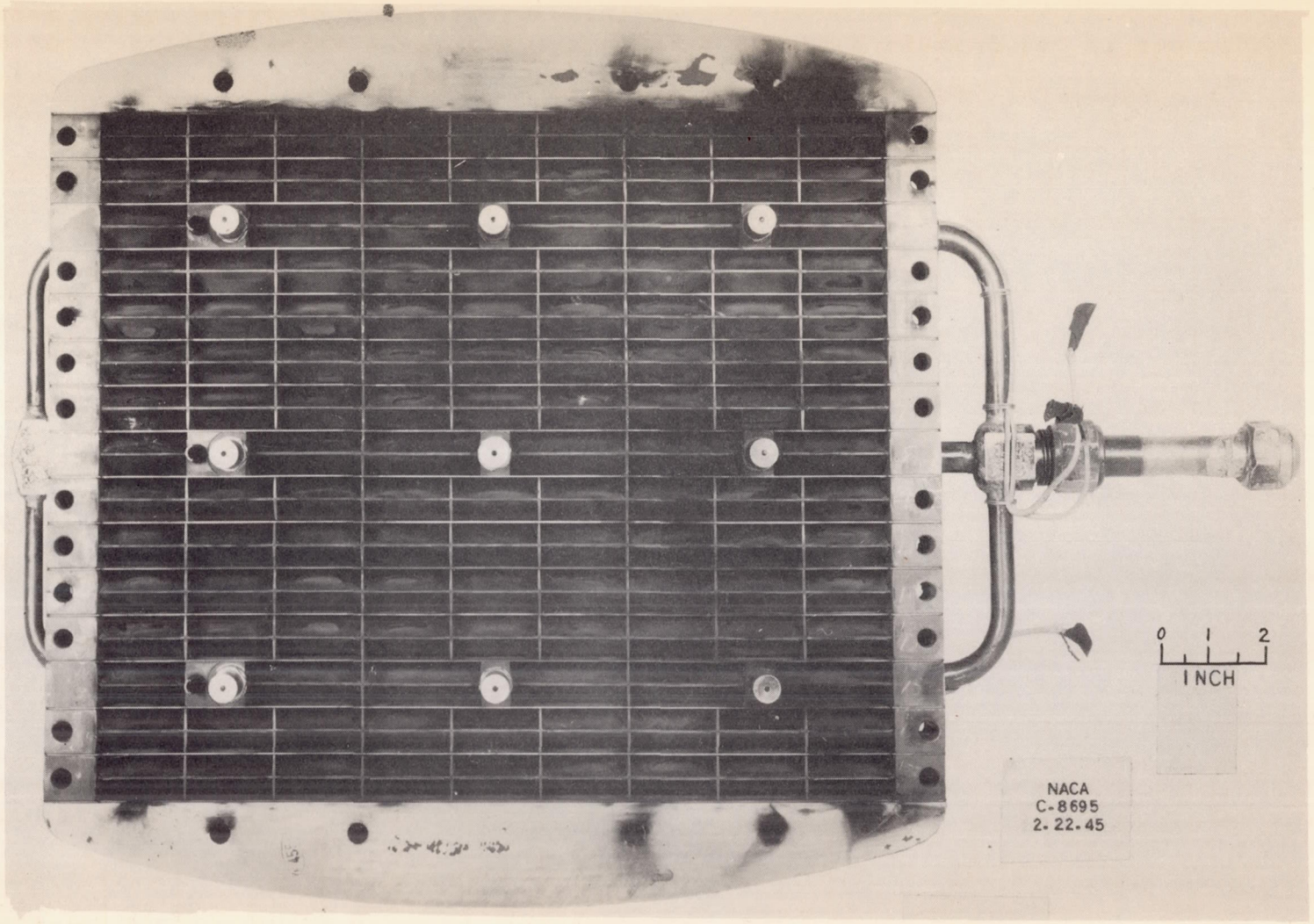

Figure 19. - Flapper-valve grid assembly after 30 minutes of operation.

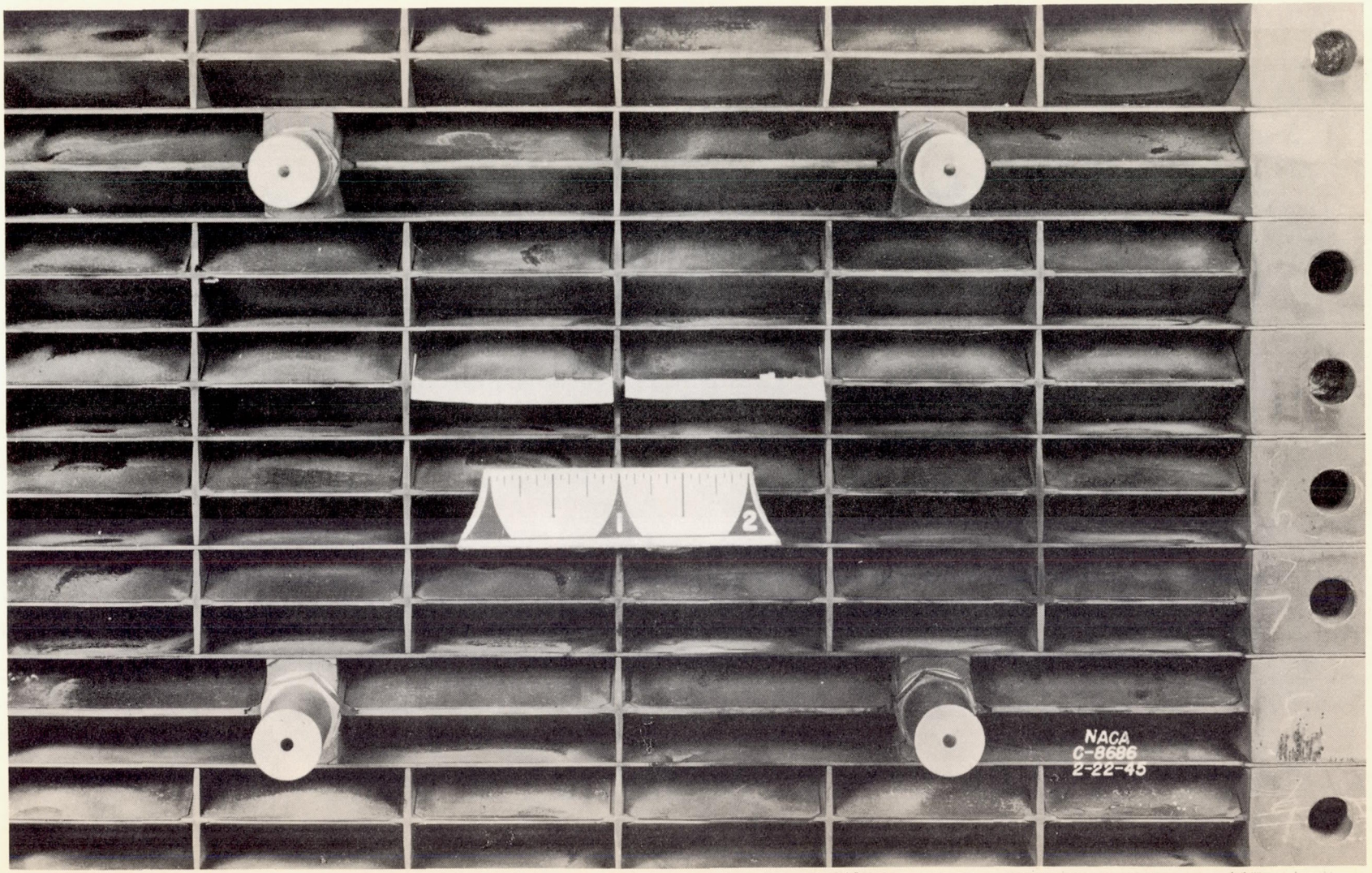

Figure 20. - Close-up view of flapper-valve grid assembly showing two of the most damaged valves after 30 minutes of operation.